

New Approaches to the Design of Nickel, Cobalt, and Nickel–Cobalt Catalysts for Partial Oxidation and Dry Reforming of Methane to Synthesis Gas

I. I. Moiseev^{a, b, c}, A. S. Loktev^{a, b, c, *, **}, O. A. Shlyakhtin^d, G. N. Mazo^d, and A. G. Dedov^{a, b, c}

^aGubkin Russian State University of Oil and Gas (National Research University), Moscow, 119071 Russia

^bKurnakov Institute of General and Inorganic Chemistry, Russian Academy of Sciences, Moscow, 119991 Russia

^cTopchiev Institute of Petrochemical Synthesis, Russian Academy of Sciences, Moscow, 119071 Russia

^dMoscow State University, Moscow, 119991 Russia

*e-mail: genchem@gubkin.ru

**e-mail: al57@rambler.ru

Received August 7, 2019; revised August 25, 2019; accepted September 6, 2019

Abstract—New approaches to the formation of active, selective, and stable Ni, Co, and Ni–Co catalysts for partial oxidation and dry reforming of methane into synthesis gas (a mixture of hydrogen and carbon monoxide) are considered.

Keywords: synthesis gas, partial oxidation of methane, dry reforming of methane, nickel, cobalt, perovskite-like oxides, mesoporous materials, zeolites, magnesium–aluminum hydrotalcite

DOI: 10.1134/S0965544119130115

INTRODUCTION

The selective catalytic reforming of methane to synthesis gas (syngas) is a key stage in the production of a variety of petrochemicals and alternative fuel components from natural gas [1–11]. According to experts, it is the syngas manufacturing process that drives about 70% of costs in the chain of production of petrochemicals from methane. Any improvement in the syngas production process is a desirable task. Teams of leading world and Russian research centers are permanently working on its solution.

The main industrial process for producing synthesis gas—steam methane reforming—is highly endothermic and, as a result, energy-consuming. The resulting syngas with a ratio of $H_2/CO = 3$ cannot be directly used for the production of petrochemicals. A more convenient composition of the synthesis gas is achieved in the processes of methane dry reforming—($H_2/CO = 1$) or partial oxidation—($H_2/CO = 2$). The latter process is also less energy consuming due to exothermicity.

The embodiment of the process of dry reforming of methane (DRM) has attracted increasing attention of researchers around the world, since two main greenhouse gases carbon-dioxide and methane- are utilized in this process. This, in turn, contributes to solving the problem of global warming. In addition, the DRM process is considered as a promising way to obtain pet-

rochemical products from the renewable feedstock biogas [12].

However, the realization of partial oxidation and dry reforming of methane into the industry is largely hampered by the lack of appropriate stable and selective catalysts. The implemented process of partial oxidation of methane (POM) proceeds as a noncatalytic reaction above 1100°C [1–3].

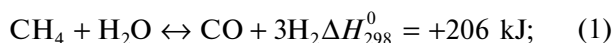
Known POM and DRM catalysts contain active sites formed by Group VIII metals, mainly nickel [1–11]. Numerous data on the use of catalysts based on platinum group metals are mainly of theoretical interest due to their high cost. At the same time, nickel catalysts are capable of catalyzing the formation of carbonaceous deposits (especially during the DRM process) and, in addition, are prone to strong interaction with the support, which can cause the formation of compounds that are inactive in catalysis. To overcome these drawbacks, catalysts are often promoted with platinum group metals, which significantly increase their cost. In some cases, it is possible to increase the stability of nickel catalysts by doping with cobalt or other nonprecious metals; however, their activity is often reduced.

A significant number of research papers and review articles are published annually on the search for new approaches to the design of active, selective, and stable POM and DRM catalysts of various natures. In this

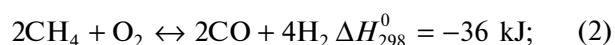
article, we restrict ourselves to considering approaches based on the improvement of certain nickel, cobalt, and nickel–cobalt mixed oxide catalysts based on perovskite and perovskite-like structures, as well as on the use of nickel, cobalt, and nickel–cobalt catalysts dispersed in a matrix of mesoporous materials, microporous materials such as zeolites, and layered aluminum–magnesium complex oxides with the hydrotalcite structure. By using these approaches, it is generally possible to obtain catalysts that hold promise for the practical implementation of the POM and DRM processes.

ON THE FEATURES OF THE POM AND DRM PROCESSES

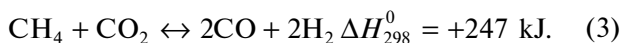
Three main processes for the oxidative conversion of methane to synthesis gas [1–11] are steam methane reforming (SMR)



partial oxidation of methane (POM)



dry reforming of methane (DRM)



The processes are characterized by different thermal effects and different compositions of the resulting syngas. The ratio of H₂ and CO, preferred for the synthesis of certain compounds, is achieved by varying the nature of the oxidizing agent or mixtures thereof. In the steam methane reforming reaction (SMR), a syngas of the CO : H₂ = 1 : 3 composition is formed, which contains a large amount of hydrogen and is used to produce ammonia.

For the synthesis of methanol or the Fischer–Tropsch hydrocarbon (HC) synthesis, the syngas with a CO : H₂ ratio of 1 : 2 is preferred (reaction (2)). That is, POM is the most preferable reaction for obtaining synthesis gas of this ratio. By the dry reforming of methane (DRM), it is possible to get syngas with the composition CO : H₂ = 1 : 1, which is favorable for the synthesis of dimethyl ether and hydroformylation reactions. Methane conversion by the action of several oxidizing agents—H₂O, O₂, and CO₂ [13, 14]—makes it possible to vary the composition of the resulting synthesis gas and the heat of the process.

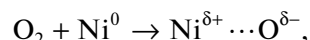
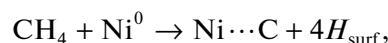
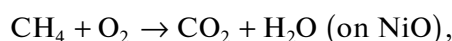
Steam and dry methane reforming are strongly endothermic reactions, whereas the partial oxidation of methane with oxygen is an exothermic reaction, so that it can be carried out in the autothermal mode. According to thermodynamic calculations, in all three processes, acceptable degree of CH₄ conversion and selectivity for CO and H₂ can be achieved only at temperatures above 800°C [15]. In addition to thermodynamic limitations, the achievement of high selectivity

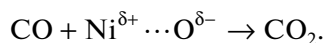
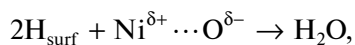
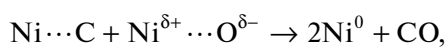
and high syngas yield is constrained by factors associated with occurrence of some thermodynamically favorable side reactions. In general, all the three modes of the oxidative conversion of methane to synthesis gas are high-temperature processes that occur efficiently in the presence of Group VIII metals.

The complete noncatalytic conversion of a mixture of methane and oxygen into synthesis gas is possible at 800–900°C and atmospheric pressure [9]. However, such high degrees of conversion under these conditions are frequently unattainable in practice because of kinetic constraints on the reforming of methane. This is due to the high energy required to activate this molecule: the homolytic dissociation energy of the H₃C–H bond is about 440 kJ/mol [16].

The first report on the catalytic oxidation of methane with oxygen in 1929 [17] describes the use of metallic nickel mixed with Al₂O₃, which made it possible to obtain synthesis gas with 78% CO selectivity at 1000°C and a methane conversion of about 90%. Similar nickel catalysts were used for steam methane reforming. To date, it has been established that systems containing Ni, Co, Ir, Pd, Pt, Ru, or Rh have catalytic activity in the POM and DRM reactions [1–15]; there are also examples of the use of Fe and Cu [9, 18]. Typically, POM and DRM catalysts are composites containing the above elements in the form of a metal or metal oxide phase dispersed on the surface or in an oxide support matrix. The support must have thermal stability in the operating temperature range of POM and DRM. In most studies, Al₂O₃, MgO, and SiO₂ are used as supports [1–25]. Rare earth oxides, such as La₂O₃, and titania, zirconia, thoria, AlPO₄ and Ca₃(PO₄)₂ are also described as supports [26–34].

Today, the mechanism of partial oxidation of methane to syngas is still under debate. Two main mechanisms, one-step and two-step, are discussed [1–10]. The former involves the direct oxidation of the methane molecule with active oxygen to produce hydrogen and carbon monoxide. In the two-step process, the initial deep oxidation is assumed to give carbon dioxide and water, which then react with an excess of methane to form the target product. Based on the results of experiments in a pulsed reactor, the temperature-programmed surface reaction (TPSR), and measurements of the temperature profile of the catalyst bed, the following sequence of POM steps on a NiO/Al₂O₃ catalyst was proposed [35]:



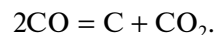


On NiO, methane is initially oxidized to carbon dioxide and water, leading to an increase in temperature in the catalyst bed. Then, at a certain temperature, along with the deep oxidation process, CH₄ reduces NiO to metallic Ni⁰, resulting in a slight decrease in temperature in the reaction zone due to the endothermic nickel oxide reduction process. At the Ni⁰ sites generated, CH₄ dissociates to give H₂ and form Ni–C bonds. Then, Ni–C intermediates can react with Ni^{δ+}⋯O^{δ-} groups, which are formed as a result of activation of gaseous O₂, leading to the formation of CO. Presumably, the formation of carbon monoxide is a rate-limiting step in this case. Studying POM on Ni/Al₂O₃, Rodrigues et al. [36] came to the same conclusion. Thus, attribution of the POM process to a particular mechanism depends on the chemical nature and the oxidation state of the active metal; and the possible presence of reactive oxygen species generated by active sites or, in some cases, provided by the crystal lattice of the oxide support. According to Au et al. [37], nickel oxide can directly act as a supplier of active oxygen. At the same time, it was shown in [29, 38] that the selective formation of carbon monoxide on the Ni/CeO₂ catalyst is due to methane dissociation on nickel metal particles, migration of active carbon particles to the interface between Ni and CeO₂, and carbon oxidation to CO by ceria lattice oxygen. It is on the CeO₂ surface that oxygen activation occurs in this case. It was shown [39–42] that in the presence of Ni/La₂O₃, methane is completely oxidized on the surface of lanthanum oxide and the conversion of the products of complete oxidation to synthesis gas proceeds on metallic nickel. Thus, the stages of oxygen activation in catalysts of this type are spatially separated. Due to the significant exothermic effect of the complete methane oxidation reaction ($\Delta H^0 = -890.3$ kJ), so-called “hot spots” can be formed, which are catalyst zones whose temperature is 100–200°C higher than the temperature in the reactor. This may be due not only to the low efficiency of heat removal by the gas stream, but also to the aforementioned microstructural features of the catalyst, which are associated with the heterogeneity of the distribution of active sites in the composite [1].

The stability of POM catalysts is determined by two main factors. One of them is the nature of the support used. It is known [1–10] that prolonged use of the Ni/Al₂O₃ catalyst in POM is accompanied by the formation of inactive spinel: NiO + Al₂O₃ → NiAl₂O₄. The presence of “hot spots” in the catalyst bed may also contribute to this process. This problem can be solved both by maintaining the reaction temperature

at which the catalyst components do not interact and by selecting a support that is inert with respect to the active phase of the catalyst in a wide temperature range. It should be noted that the growth in size of the metal particles of the catalyst at high temperatures leads to a decrease in its active surface area and a decline in specific activity of the material. For example, it was shown [43] that an increase in size of rhodium metal nanoparticles from 1.1 to 5.5 nm reduces the yield of syngas in the POM reaction from 85 to 60%.

However, the main reason for the deactivation of POM catalysts in most cases is catalyst coking [1, 32, 44]. The formation of carbon deposits can occur according to the Boudouard reaction, proceeding at a noticeable rate at 700–800°C:



The carbon produced, as a rule, forms porous structures between catalyst particles; these structures do not have a noticeable effect on the catalytic activity.

The second route of coking involves the dissociation of methane on the surface of metal particles. In this case, carbon is produced in the form of dense layers, which impede the access of gas molecules to active sites and noticeably reduce catalytic activity up to its complete loss. According to [44], coking intensity decreases in the order Ni > Pd > Rh > Ru > Pt, Ir. Cobalt-containing catalysts are also less susceptible to deactivation by coking [1]. High-temperature pyrolysis of methane can also contribute to the formation of carbon deposits.

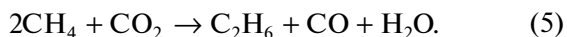
Bhavani et al. [33] carried out partial oxidation of methane on Ni/Al–Ce–ZrO₂ and found that the rate of formation of dense carbon layers depended on the size of nickel particles. Carbon atoms C_{ads} formed as a result of methane dissociation are involved in the parallel processes of the formation of the covalent C–C bond and the buildup of a carbon phase layer on the surface of nickel particles, as well as in migration to the Ni/support interface and oxidation by lattice oxygen to give CO or CO₂. In the case of a large size of metal particles, the concentration of surface carbon is higher and the rate of formation of the dense carbon phase is greater than the carbon oxidation rate. However, if the particle size of the metal is sufficiently small and, accordingly, its specific surface area is large, then the oxidation process can prevail over coke formation due to more efficient contacting of carbon and oxygen particles on the metal surface. Thus, control of the particle size of the catalyst can enhance its stability.

As in the case of POM, nickel catalysts are most active in DRM. Catalysts based on Co, Fe, Pt, Pd, Rh, and Ir [1–10, 12–15] supported on various carriers are less commonly used. It is noted that basic supports (MgO, La₂O₃, etc.) are able to participate in the activation of adsorbed CO₂, which reacts with carbon via the reverse Boudouard reaction.

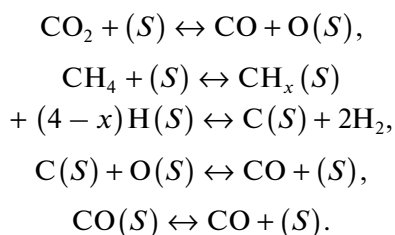
Compared to steam reforming, DRM is an even more endothermic process. Selectivities and conversions close to 100% are achieved at 1000–1100°C, although the Gibbs free energy is zero at 640°C. Below this temperature, CO methanation intensively proceeds and the equilibrium shifts toward the formation of CH₄ and CO₂. Along with the main reaction (3), carbon formation can occur in a mixture of CH₄ and CO₂:



In addition, oxidative coupling of methane can occur under the influence of CO₂:



In [45–47], the mechanism of the DRM reaction was substantiated, including the steps of the formation of adsorbed C, H, O, and CO particles on the surface (*S*) of DRM catalysts, which subsequently produce CO and H₂:



In studies [48–50] at the Institute of Chemical Physics, Russian Academy of Sciences, it was shown that the main route of DRM on Ni/ α -Al₂O₃ and Co/ α -Al₂O₃ catalysts includes methane chemisorption with the formation of C + 2H₂, as well as the interaction of carbon with CO₂ by the reverse Boudouard reaction. Methane practically does not react with nickel and cobalt oxides, but actively interacts with reduced metals, forming H₂ and surface carbon, which, in turn, slowly reacts with lattice oxygen and is able to react quickly with surface-bound oxygen. Surface carbon also reacts rapidly with CO₂ to form CO and slowly with metal (Me) particles to form CO and MeO.

Side routes are the interaction of chemisorbed C and H₂ with catalyst lattice oxygen and the dissociative adsorption of CO₂ on the metal. The competitive reaction of surface carbon with surface-bound oxygen decreases the conversion of CO₂ in the main reaction; therefore, the addition of O₂ causes a decrease in the rate of the reaction CH₄ + CO₂ (catalyst poisoning with oxygen). However, the main problem of nickel-containing DRM catalysts is the activity loss due to coking [1–10]. The surface carbon particles formed in the presence of nickel catalysts are actively involved in the growth of carbon fibers and dense carbon layers accompanied by catalyst deactivation.

In the following sections, we analyze approaches to the design of nickel, cobalt, and nickel-cobalt catalysts

for POM and DRM, leading to enhancement of their activity, selectivity, and stability.

PEROVSKITE-LIKE NICKEL, COBALT, AND NICKEL–COBALT CATALYSTS FOR POM AND DRM PROCESSES

The use of various complex oxide systems based on perovskites; aluminates; or compounds with the structure of fluorite, pyrochlore, etc. in catalysis of POM and DRM attracts the attention of researchers [1–10, 28, 51–57], since high activity, selectivity, and stability in POM and DRM can be achieved in this way as a result of the formation of a highly dispersed nickel and/or cobalt metal phase stabilized by oxides of rare earth and some other elements.

Among these compounds, catalysts with a perovskite structure are distinguished [58–64]. Perovskites, compounds of the general formula ABO₃, are characterized by a crystal structure containing octahedral BO₆ units. The octahedra are interconnected through common vertices, forming endless chains in three mutually perpendicular directions. In the model of the closest spherical packings, the ABO₃ perovskite structure can be described as the closest cubic packing formed by the atoms of oxygen and element A, in which the B atoms occupy the octahedral voids. In the case of an ideal cubic structure, cation A has cubic octahedral coordination with a coordination number of 12. The radius of cation A in the perovskite structure should be larger than that of cation B, as characterized by the Goldschmidt relation:

$$\sqrt{2}(r_B + r_O) = (r_A + r_O),$$

in which r_A , r_B , and r_O are the radii of cations A, B, and oxygen, respectively.

There are many known compounds that do not satisfy this relation but have a perovskite structure. Their cubic lattice is distorted because of an increase in the difference of the radii of the ions. This distortion is described by Goldschmidt's tolerance factor t : $t = (r_A + r_O)/\sqrt{2}(r_B + r_O)$.

The perovskite structure is preserved at t from 0.86 to 1.1 [65].

Catalysts with a perovskite structure are actively studied in oxidative processes, including the POM and DRM processes. In this review, we do not consider numerous publications on syngas production from methane using oxygen-conducting membranes based on perovskite-like materials [2, 61]. These systems make it possible to combine the syngas generation and air separation processes, eliminating expensive equipment for oxygen production from the process flow chart. However, the commercialization of POM membrane reactors is hindered by the problems of their insufficient resistance to poisoning, corrosion, deformation, and high differential pressure. In addition, methane conversion and synthesis gas selectivity

in this case are limited by oxygen diffusion inside the membrane, which affects the extremely low productivity of such materials. For these reasons, we restrict ourselves to considering the use of perovskite-like materials as ordinary heterogeneous catalysts.

Zirconates and hafnates with the perovskite structure obtained by partial replacement of strontium or barium by nickel ($\text{Sr}_{0.8}\text{Ni}_{0.2}\text{ZrO}_3$, $\text{Sr}_{0.8}\text{Ni}_{0.2}\text{HfO}_3$, $\text{Ba}_{0.8}\text{Ni}_{0.2}\text{ZrO}_3$) were comparable in activity in POM with a catalyst containing metallic nickel [66]. A nitrogen-diluted 2 : 1 mixture of methane and oxygen was used. Undoped SrZrO_3 exhibiting no noticeable activity. According to X-ray diffraction (XRD) analysis, there was no chemical degradation of perovskites or significant change in their structure. The catalysts were resistant to coking, retaining catalytic activity for 70 h. The authors attribute the absence of noticeable coking to the fact that nickel atoms are integrated into the perovskite crystal lattice.

In the case of POM catalysis by $\text{LaNi}_{1-x}\text{Fe}_x\text{O}_3$ solid solutions ($x = 0-1$) [67], the catalysts underwent conversion into a mixture of lanthanum oxide, nickel oxide, and a phase with a perovskite structure having the iron predominantly in the B position. The catalytic properties of the resulting composites correlate with the cationic composition of perovskites formed. The composites do not exhibit noticeable activity when LaFeO_3 and $\text{LaFe}_{0.9}\text{Ni}_{0.1}\text{O}_3$ are formed, whereas in the case of perovskites with a high nickel content, the formation of CO occurs at 900°C with a yield of about 90%. Provendier et al. [67] attribute the increase in the yield of POM products to the presence of the Ni^0 phase in the composite.

Enhancement of catalytic activity in POM as a result of the reductive decomposition of $\text{LaNi}_{1-x}\text{Co}_x\text{O}_3$ perovskites and the formation of composites in which metal particles uniformly dispersed in the oxide matrix was also reported in [55]. The formation of a Co–Ni alloy during the reduction process was noted. That is, compounds of POM-active 3d metals with a perovskite structure can be considered as precursors of catalytically active composites formed by reductive degradation, although this contradicts the results of the above-cited study [66], according to which the perovskite precursor does not decompose during the POM process.

Perovskites containing cobalt and iron, such as LaCoO_3 , LaFeO_3 , and $\text{LaCo}_{0.5}\text{Fe}_{0.5}\text{O}_3$, were inactive in POM at 700°C even after preliminary reduction in H_2 [68]. At the same time, when $\text{LaNi}_{1-x}\text{Co}_x\text{O}_3$ solid solutions ($x = 0, 0.3, 0.5, 1$), previously reduced with hydrogen, were used in POM, an increase in the proportion of nickel leads to an increase in methane conversion and selectivity for CO and H_2 [69]. In addition, hydrogen temperature-programmed reduction (TPR) of the aforementioned perovskites has shown that the replacement of nickel by cobalt is accompanied by a shift in the H_2 absorption maxima to higher

temperatures, which may be due to the greater stability of cobalt-containing perovskites [70]: $\Delta_f H_{298}^0 \text{LaCoO}_3 = -1241 \text{ kJ/mol}$, $\Delta_f H_{298}^0 \text{LaNiO}_3 = -1192 \text{ kJ/mol}$. The perovskite LaFeO_3 , inactive in POM, is even more stable, its $\Delta_f H_{298}^0 = -1373 \text{ kJ/mol}$. More stable perovskites are characterized by a higher Goldschmidt tolerance factor and are less active in POM. According to [71], it is the resynthesis of compounds with perovskite structure that is responsible for the loss of POM activity of the reduction products of LnCoO_3 perovskites ($\text{Ln} = \text{La, Pr, Nd, Sm, Gd}$).

It was shown [28] that perovskite-like Co- and Pt-substituted lanthanum nickelates are significantly less active and selective in POM compared with 5% Ni/ $\gamma\text{-Al}_2\text{O}_3$, which retains the values of CH_4 conversion and selectivity for CO and H_2 at a 90% level even with increasing volumetric flow rate. Based on XRD and thermogravimetric data, Veila et al. [28] hypothesized that the low catalytic activity may be associated with the formation of a low-active La(OH)_3 phase.

At the same time, perovskite $\text{Ca}_{0.8}\text{Sr}_{0.2}\text{Ti}_{1-y}\text{Ni}_y\text{O}_3$ catalyzed the deep oxidation of methane at 600°C and, with an increase in temperature to 800°C , the formation of synthesis gas. An increase in the degree of substitution y from 0.1 to 0.2 increased the activity in both reactions [72].

It was shown [73] that during the POM, the perovskite-like structure of LaMO_3 ($\text{M} = \text{Rh, Ni, Co}$) is decomposed to La_2O_3 and the metal phase of the transition elements. The most active and stable catalyst was formed by LaRhO_3 decomposition products: a methane conversion of 95% and CO selectivity of 98% remained stable for 120 h. The products of LaNiO_3 decomposition were deactivated after 17 h on stream, probably, because of coking. The LaCoO_3 -based catalyst mainly resulted in deep oxidation products, but it was reduced after 30 h on stream to Co^0 dispersed in the La_2O_3 matrix, after which the reaction shifted toward the formation of CO and H_2 .

According to Toniolo et al. [74], the partial replacement of Co in LaCoO_3 by Cu ions made it possible not only to prevent coke deposition and the subsequent deactivation of the catalyst, but also to lower POM temperature.

The $\text{LaNi}_{1-x}\text{Fe}_x\text{O}_3$ ($x = 0-1$) POM catalysts described in [67] were also active in DRM. On a composite formed from $\text{LaNi}_{1-x}\text{Fe}_x\text{O}_3$, 100% conversion of CH_4 and CO_2 was achieved at 800°C [75]. As in the POM process, the perovskite-like structure of the catalyst was destroyed; Ni–Fe alloys formed at $x = 0.3-0.8$. The authors believe that the formation of alloys prevents catalyst poisoning with carbon by inhibiting carbon diffusion through Ni particles. Less active catalysts are obtained by supporting such perovskites on silica [76]. Composites formed during the DRM pro-

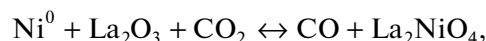
cess consist of individual oxides and silicates of perovskite-forming elements.

Perovskite-like DRM catalysts $\text{La}_{1-x}\text{Sr}_x\text{NiO}_3$ and $\text{La}_{2-x}\text{Sr}_x\text{NiO}_4$ were studied in [77]. The maximum activity was observed for $\text{La}_{0.9}\text{Sr}_{0.1}\text{NiO}_3$ and $\text{La}_{1.8}\text{Sr}_{0.2}\text{NiO}_4$. According to XRD data, catalysts turn into a mixture of $\text{La}_2\text{O}_2\text{CO}_3$, SrCO_3 , and metallic Ni under DRM conditions. It was suggested that the high activity of the catalysts is due to the presence of CO_2 -activating La_2O_3 and CH_4 -activating Ni.

Santos et al. [78] found that the POM results depend on the procedure for reducing lanthanum–nickel–cobalt perovskite. The reduction of $\text{LaNi}_{1-x}\text{Co}_x\text{O}_3$ perovskites ($x = 0.0, 0.2, 0.5,$ and 1.0) with hydrogen resulted in the formation of $\text{La}_2\text{M}_2\text{O}_5$ ($M = \text{Ni}$ and Co), which then transform into $\text{Ni}_{1-x}\text{Co}_x/\text{La}_2\text{O}_3$. At the same time, during the reduction of $\text{LaNi}_{0.8}\text{Co}_{0.2}\text{O}_3$ with a $\text{CH}_4 + \text{O}_2$ mixture, La_2MO_4 spinel ($M = \text{Ni}$ and Co) was initially formed, which also transformed into $\text{Ni}_{1-x}\text{Co}_x/\text{La}_2\text{O}_3$. Preliminary reduction with hydrogen led to the formation of smaller nickel crystallites, which catalyze the production of synthesis gas with $\text{H}_2/\text{CO} = 2$. In the absence of prereduction, a composite was formed that significantly catalyzed the reverse water-gas shift reaction, leading to the production of syngas with $\text{H}_2/\text{CO} = 1.6$.

According to Jang et al. [79], it is with the use of perovskite-based catalysts that highly dispersed stable nickel DRM catalysts can be obtained. Testing of the LaNiO_3 perovskite in a DRM puls reactor after hydrogen reduction showed that syngas formation started at 700°C and 100% CH_4 conversion and 92% CO_2 conversion were achieved at 800°C . At 800°C , catalyst

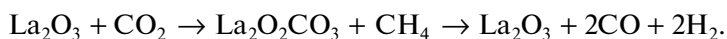
consisted of La_2O_3 and metallic nickel, whereas it contained spinel La_2NiO_4 at 700°C [80]. This finding was assumed to be evidence for the occurrence of DRM according to the scheme:



High stability of the LaNiO_3 perovskite reduction products in DRM was noted in [81]. A catalyst regeneration method by reoxidation to perovskite and repeated reduction was proposed. The instability of the catalyst in steam reforming was noted, and it was associated with the oxidation of nickel particles in the presence of water.

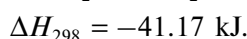
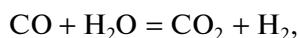
The presence of manganese ions in $\text{LaNi}_{1-x}\text{Mn}_x\text{O}_3$ perovskites ($x = 0, 0.2, 0.4, 0.6, 0.8,$ and 1.0) increases the temperature of Ni^{3+} reduction to Ni^0 , thereby leading to an increase in the number of nanosized Ni^0 particles in the $\text{MnO}_x\text{--La}_2\text{O}_3$ matrix [82]. Perovskites with $x \leq 0.8$ turned out to be more active and stable in DRM because of the formation of Ni^0 dispersed in the $\text{La}_2\text{O}_2\text{CO}_3\text{--MnO--Mn}_2\text{O}_3$ matrix.

Over $\text{LaNi}_{1-x}\text{Co}_x\text{O}_3$ (x from 0 to 1) DRM catalysts that were not subjected to preliminary hydrogen reduction, the syngas yield increased with increasing temperature from 600 to 800°C , the enhancement being associated with the formation of active components as a result of the reduction of the initial perovskites [83]. The catalysts with $x < 0.6$ were less active. The inhibition of catalyst coking was associated with the formation of solid solutions of cobalt and nickel metal nanoparticles, as well as with the presence of lanthanum oxide, which facilitates the reactions:



A similar effect of lanthanum oxide in the case of POM catalysis was noted in [77].

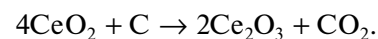
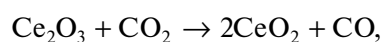
Valderrama et al. [83] found that the $\text{La}_2\text{O}_2\text{CO}_3$ phase does not form in the absence of nickel and that hydrogen-rich synthesis gas is produced at $x \leq 0.6$ via the following reactions:



Partial replacement of lanthanum by strontium (catalysts based on $\text{La}_{1-x}\text{Sr}_x\text{Ni}_{0.4}\text{Co}_{0.6}\text{O}_3$ and $\text{La}_{0.8}\text{Sr}_{0.2}\text{Ni}_{1-y}\text{Co}_y\text{O}_3$ perovskites) facilitates the formation of Ni^0 and Co^0 nanoparticles dispersed in the matrix formed by $\text{La}_2\text{O}_2\text{CO}_3$ and SrO in the DRM process; these particles catalyze DRM and are not prone to coking [84]. The introduction of strontium

makes it possible to obtain active and stable DRM catalysts based on nickel-free $\text{La}_{1-x}\text{Sr}_x\text{CoO}_3$ [85].

In the series of perovskites obtained by the partial replacement of lanthanum with cerium ($\text{La}_{1-x}\text{Ce}_x\text{NiO}_3$, $x = 0.05, 0.4, 0.7$) [86], the most active DRM catalyst was the one based on $\text{La}_{0.95}\text{Ce}_{0.05}\text{NiO}_3$, which contained highly dispersed nickel metal. The cerium-free catalyst was less stable. At a higher cerium content, a composite containing CeO_2 , NiO , and La_2NiO_4 was formed instead of the perovskite structure. The authors attribute the coke resistance of the catalyst to the occurrence of the reactions:



The use of complex perovskite-like oxides of 3d elements with the general formula A_2BO_4 belonging to the K_2NiF_4 structural type as POM and DRM

catalyst precursors also attracts increasing attention of researchers. This structure can be described as an alternation of AO and BO₂ layers in a 2 to 1 ratio along the crystal lattice parameter *c* [87]. The interest in these compounds is largely due to their unusual magnetic properties and high mobility of oxygen ions in the crystal lattice [88–94].

As noted above, in this review we do not consider numerous publications on syngas production using oxygen-permeable membranes and confine ourselves to the use of materials of this kind as ordinary heterogeneous catalysts. An example of such a compound having special electrophysical and high-temperature properties is NdCaCoO₄ with the structure of tetragonal K₂NiF₄ [93]. Materials based on it turned out to be active POM and DRM catalysts [11, 95–98]. In the POM reaction at 920°C, 100% selectivity for CO was achieved at a methane conversion of 90%. These characteristics did not decline for 140 h. During the POM process, NdCaCoO₄ is decomposed to give Nd₂O₃, CaO, CoO, and metallic cobalt.

LaSrCoO₄ appeared to be more resistant to reduction than NdCaCoO₄ and less active in catalysis [96]. This difference is due to the larger ionic radii of La³⁺ (1.22 Å) and Sr²⁺ (1.31 Å) compared to Nd³⁺ (1.16 Å) and Ca²⁺ (1.18 Å), respectively, which should ensure a more stable structure according to the Goldschmidt model and complicate the formation of a catalytically active composite.

High activity of the NdCaCoO₄ degradation products was achieved at temperatures above 920°C, but the introduction of nickel can significantly reduce the POM and DRM temperature [54, 55, 69]. At temperatures less than 800°C, an increase in the amount of cobalt, on one hand, reduces the degree of conversion of the reactants but, on the other hand, increases the coke resistance of the catalysts by limiting the size of nickel particles.

The catalysis of partial oxidation of methane by the reduction products of single-phase Nd_{2–y}Ca_yCo_xNi_{1–x}O₄ complex oxides having the K₂NiF₄ structure was studied in [99]. The ability of the obtained mixed Ni–Co catalysts to provide comparatively high syngas yields below 850°C indicates that not only metal nanoparticles, but also resynthesis products—phases of complex oxides—can participate in the catalytic POM and DRM processes.

An analysis of the studies surveyed in the review [100] on the use of perovskite-like catalysts in DRM shows that the most active and stable catalysts contain nickel and rare-earth ions, and the synthesis of starting materials is rather complicated, whereas the actual POM and DRM catalysts are almost always the products of the decomposition of the materials in question to oxides and metals. In [101], it was proposed to obtain POM and DRM catalysts by the accelerated method, without achieving the formation of a single-

phase precursor. The nitrates of cobalt, nickel, neodymium, and calcium oxide taken in the required ratios were dissolved in water, followed by evaporation, drying, and calcination for 5 h at 900°C. The reactant ratio simulated the composition of perovskites and perovskite-like materials of the K₂NiF₄ structural type. The multiphase material similar in composition to NdCaCoO₄ studied in [11, 95–98] showed in POM a methane conversion of 98% and selectivities for CO and H₂ of 96 and 98%, respectively, already at 890°C. A calcium-free material, corresponding to the composition of NdCoO₃, provided 90% methane conversion and CO and H₂ selectivity of 93 and 100%, respectively, already at 860°C. The complete replacement of Co by Ni resulted in a more active POM catalyst. At 775°C, the methane conversion was 92%, and the selectivity for CO and H₂ was 91%. The mixed Nd–Co–Ni catalyst at 800°C showed a methane conversion of 92%, a CO selectivity of 94%, and an H₂ selectivity of 98%, not inferior to the nickel-containing sample. In the DRM reaction, the nickel catalyst at 850°C showed a methane conversion of 97%; a CO₂ conversion of 98%; and CO and H₂ yields of 98 and 97%, respectively. The mixed Nd–Co–Ni catalyst showed the same results in DRM at 880°C.

The catalyst NdNiCoO₄ discussed in [100] contained 18 wt % Ni and Co. Other well-known perovskite and perovskite-like POM and DRM catalysts also contain significant amounts of nickel and cobalt, more than 2 wt %. A high nickel content can affect the stability of the catalysts, leading to the formation of larger nickel particles prone to coking. Indeed, after 50 h on stream in POM at 920°C, the NdNiCoO₄ catalyst described in [100] lost its activity, the graphite phase appeared in its composition, and microphotographs showed the presence of carbon deposits [102]. Thus, the stability of nickel-containing POM and DRM catalysts is achieved in the case of maintaining a small size of nickel particles during long-term operation. In [33, 43], a decline in catalyst activity with an increase in the size of metal particles was noted. Stable perovskite catalysts are formed by introducing small amounts of nickel [33] or in the presence of REE oxides, for example, cerium oxide, promoting the oxidation of carbon [86]. The stability of the catalysts is also ensured by the selection of a support that does not bind metal particles into inactive phases and facilitates their preservation in a finely dispersed state.

MESOSTRUCTURED NICKEL, COBALT, AND NICKEL–COBALT POM AND DRM CATALYSTS

The use of heterogeneous catalysts with a mesoporous structure in the catalysis of POM and DRM is considered an effective approach to increasing activity, selectivity, and stability [100].

Gonzalez et al. [103] used Ni, Co, and Ni + Co catalysts introduced by impregnation into a mesoporous silicate material containing channels of about 2.5 nm in diameter for DRM catalysis. The most active, selective, and stable material was found to contain 10 wt % Co and 15 wt % Ni. At 700°C and with the nitrogen-diluted reactants, the hydrogen-reduced catalyst showed a methane conversion of 72%; a CO₂ conversion of 74%; and CO and H₂ selectivities of 85 and 78%, respectively. Under similar conditions, the LaCo_{0.4}Ni_{0.6}O₃ perovskite-based catalyst turned out to be more active, but less selective for hydrogen to ensure a methane conversion of 91%; a CO₂ conversion of 99%; and CO and H₂ selectivities of 89 and 27%, respectively. The researchers associated the results with the occurrence of the Boudouard reaction and the reverse water-gas shift reaction. Both catalysts underwent coking, but the perovskite-based catalyst had an on-stream stability of 100 h, demonstrating the above results.

A hydrogen-reduced 10 wt % NiO/TiO₂-SiO₂ (50 : 50) mesoporous material with a pore diameter of 14 nm, synthesized using the template-free sol-gel method, showed stable CH₄ and CO₂ conversions of 88 and 97% for 30 h at atmospheric pressure and 850°C [104]. The catalyst stability was attributed to the formation of the Ni_{2.44}Ti_{0.72}Si_{0.07}O₄ phase, which prevents the sintering of nickel nanoparticles. However, carbon fibers are detected in the microphotographs of the catalyst after POM.

Damyanova et al. [105] deposited nickel and palladium on a MCM-41 mesoporous silicate support (pore diameter 3 nm). The Ni/Si ratio varied between 0.2–0.4. The DRM reaction was carried out at low temperatures, not above 550°C. Thus, the yields of hydrogen and CO on the nickel catalyst were 11 and 15%, respectively, and increased to 20 and 25% by promoting with palladium. The formation of carbon fibers was observed on both the catalysts. The particle size of nickel increased from 18 to 24 nm after POM on the monometallic nickel catalyst and from 8 to 12 nm in the case of the palladium-promoted catalyst. Therefore, deactivation of the bimetallic catalyst was slower.

The same research group [106] used alumina-supported nickel catalysts (10 wt % Ni) doped with cerium oxide (1–12 wt %) in DRM; the pore diameter of the materials was 12–14 nm. The catalysts were tested by feeding a reactant mixture diluted with nitrogen. At 550°C, the supported catalyst containing 6 wt % CeO₂ showed the maximum methane and CO₂ conversions of 57 and 69% and the hydrogen and CO yields of 29 and 46%, respectively. These parameters did not change over 6 h. Raising the temperature to 750°C increased the methane and CO₂ conversions to 90 and 98%, respectively. The catalysts after POM contained up to 3 wt % carbon, the amount of which correlated with the size of nickel particles. On the catalyst con-

taining 6 wt % CeO₂, the size of nickel particles after POM increased from 5 to 6 nm, and their size in the absence of CeO₂ increased from 6 to 8.5 nm. Accordingly, the amount of carbon in the latter sample was 7%.

The mesoporous NiO-SiO₂ catalyst, synthesized using the hydrothermal method with a structure-directing agent (pore diameter 4 nm) and characterized by uniform distribution of Ni in the silicate matrix, was tested in the DRM reaction [107]. On the catalysts with a nickel loading of 3–5 wt %, a CO₂ conversion of 90–95% and a CH₄ conversion of 93–94% were achieved at 750–800°C. After 70 h of continuous testing, the amount of carbon on the catalyst surface did not exceed 1 mmol/g of catalyst.

By impregnating foamed silicon carbide, which had mesopores of a 14 nm diameter in its structure, with an aqueous solution of nickel nitrate, a 7 wt % Ni/SiC DRM catalyst was obtained; this catalyst retained CH₄ and CO₂ conversion values at 94 and 95.0%, respectively, for 100 h at 800°C [108].

Liu et al. [109] compared the properties of DRM catalysts obtained by the introduction of nickel into the matrix of mesoporous silicates MCM-41 (pore diameter 3 nm) and SBA-15 (pore diameter 7 nm) using the conventional impregnation technique or through evaporation of a toluene solution of nickel acetylacetonate, in which these supports had been immersed. Over all the catalysts tested, methane conversion increased with increasing temperature, exceeding 90% at 800°C. The most stable catalyst was 5 wt % Ni/SBA-15 obtained from a toluene solution of nickel acetylacetonate. After 70 h on stream, the carbon content in the catalyst did not exceed 9% and the size of nickel particles was 8–9 nm. A less stable analogous catalyst based on MCM-41 contained 23% coke, despite the smaller nickel particle size of 7 nm. Liu et al. explained the result by the lower stability of the MCM-41 structure.

The catalysts of the same composition obtained by impregnating the supports with an aqueous nickel salt solution were not stable enough. Relatively high stability was observed for the 5 wt % Ni/MCM-41 catalyst containing 14-nm nickel particles and producing a large amount of coke (34%). The catalyst 5 wt % Ni/SBA-15 was less stable and formed less coke, but it contained large 31-nm nickel particles, which were deactivated as a result of formation of carbon fibers.

The 4 wt % Ni/MCM-41 DRM catalyst, containing 4-nm nickel particles formed from nickel nitrate introduced at the support synthesis step, underwent rapid coking [110]. Additional introduction of platinum in an amount of 0.8 wt % led to a stable catalyst, which retained a 90% methane conversion for 72 h at 750°C.

The introduction of Co into Ni/SBA-15 (Ni/Co = 4/1) makes it possible to reduce agglomeration of nickel

particles and catalyst coking in the DRM process due to the formation of a Ni–Co alloy [111]. At 750°C, catalyst shows methane and carbon dioxide conversion values of 73 and 89%, respectively.

Deposition of 12 wt % Ni on a SBA-15 support containing Ce ions in the crystal lattice (Ce/Si = 0.04) made it possible to obtain an active and stable DRM catalyst [100]. The presence of cerium ions increases the dispersion of nickel particles and coke resistance.

Formation of nickel–cerium (Ni/Ce = 1/1) nanoparticles in the mesopores of SBA-16 silicate made it possible to obtain a DRM catalyst with a uniform size distribution (6 nm) of nickel particles [112]. Addition of cerium facilitates the reduction of nickel to metal. Catalyst was stable in DRM at 700°C for 100 h; the authors attribute the stability to the combined effect of the mesoporous structure and the presence of cerium dioxide on the state of nickel particles.

Ni–Ce/SBA-15 catalyst (5 wt % Ni, 6 wt % Ce) [113], obtained by sequentially impregnating SBA-15 with cerium and nickel compounds, showed 100% CH₄ conversion in DRM at 650°C. The reverse order of introduction of ions worsened the catalyst properties.

In [114], a DRM catalyst was obtained by introducing cyclopentadienylnickel vapor into the cerium-containing mesoporous silicate MCM-41. The size of Ni particles was 2–4 nm. Methane conversion at 800°C was 94%, which approaches the thermodynamically equilibrium value of 96%. CO₂ conversion reached 100%. Catalyst remained stable at 750°C for 20 h with negligible coking.

The DRM reaction on a mesoporous silicate, called KIT-6, containing nickel ions introduced at the synthesis stage is described in [115]. The size of nickel particles dispersed on the surface of mesopores did not exceed 5 nm. The introduction of nickel at the synthesis step led to a significant increase in the mesopore diameter of this material from 5 to 16–17 nm. Catalysts containing 4 and 6 wt % nickel showed the same degrees of methane and CO₂ conversion of 85 and 90% at 800°C, close to thermodynamically equilibrium values. These values were retained for 180 h, which is explained by the resistance to coking of the catalyst. After 5 h on stream, the carbon content was less than 1 wt %.

In [116], a nickel compound to form stable nanosized (2–6 nm) nickel particles catalyzing DRM was introduced into SBA-15 pores as a solution in ethylene glycol. Catalyst was pyrolyzed in an inert atmosphere, which led to the formation of nickel particles dispersed in carbon in the support channels. Next, the carbon was removed by annealing in air. At 800°C, methane conversion of 90% and a CO₂ conversion of 98% were achieved. The catalyst operated stably for 20 h at 750°C, showing an 87% conversion of methane and 96% of CO₂. Such results are due to the contribution

of the reverse water-gas shift reaction. The catalyst after 20 h on stream contained 3.8 wt % coke in the form of graphite and nanotubes.

Guo et al. [117] synthesized DRM catalysts by introducing lanthanum nickelates of various compositions into the matrix of KIT-6 and SBA-15. The support was immersed in a solution of nickel and lanthanum nitrates and citric acid, dried, and calcined. La₂NiO₄/KIT-6 catalyst at 800°C and a CO₂/CH₄ = 1.1 gas mixture feed rate of 33.6 L/(g_{cat} h) showed the 100% conversion of the reactants and a syngas yield close to 100%. At 850°C, the yield of CO increased and the yield of H₂ decreased because of the reverse water-gas shift reaction. As in the case of catalysis by the same unsupported materials, the lanthanum oxide phase prevented the aggregation of nickel active centers. The catalyst based on the unique cubic structure KIT-6 was more stable in DRM than its analogue based on SBA-15, whose channel structure impeded the diffusion of the reactants and products. In addition, SBA-15 is less thermostable. Nevertheless, after 30 h of stable operation of the La₂NiO₄/KIT-6 catalyst, methane conversion noticeably decreased.

Rivas et al. [118] synthesized LaNiO₃, La_{0.8}Ca_{0.2}NiO₃, and La_{0.8}Ca_{0.2}Ni_{0.6}Co_{0.4}O₃ perovskites in the SBA-15 matrix according to a procedure similar to that described in [117]. The introduction of these complex oxides into the SBA-15 matrix led to an increase in the diameter of mesopores from 4 nm to 7, 13, and 26 nm, respectively. This change, along with the TPR data, indicates a strong interaction of perovskites with the support. All the supported catalysts turned out to be more active in DRM in comparison with the unsupported perovskites. The best results were shown by LaNiO₃/SBA-15. At 700°C, the methane and CO₂ conversions were 88 and 91%, respectively. The methane conversion did not change for 24 h.

Comparison of the DRM results on LaNiO₃, LaNiO₃/SBA-15, LaNiO₃/MCM-41, and LaNiO₃/SiO₂ catalysts [119] showed that all the supported catalysts were superior to the unsupported perovskite in activity. At 800°C, LaNiO₃/SBA-15 and LaNiO₃/MCM-41 showed a CO₂ conversion of about 80% and methane conversions of 90% and 100%, respectively. The catalyst LaNiO₃/MCM-41 underwent faster deactivation. After 60 h, the specific surface area of this catalyst decreased from 409 to 63 m²/g, the diameter of mesopores increased from 2 to 3.5 nm, and the size of nickel particles was 13 nm. In the case of more stable LaNiO₃/SBA-15, the specific surface area decreased from 246 to 76 m²/g, the diameter of mesopores increased from 4 to 5 nm, and the size of nickel particles was 8 nm. It can be seen that this catalyst has a more stable structure and nickel particles do not form large clusters.

Similar results were obtained in [120]. $\text{LaNiO}_3/\text{SBA-15}$ (specific surface area of $150 \text{ m}^2/\text{g}$) was reduced to $\text{Ni}/\text{La}_2\text{O}_3/\text{SBA-15}$ (specific surface area of $50 \text{ m}^2/\text{g}$), which catalyzed DRM at 800°C , showing a conversion of the reactants close to 90% and practically not coking for 48 h at 700°C .

In [121], DRM was carried out over mesoporous $\text{NiO-Al}_2\text{O}_3$ catalysts obtained by template synthesis from a gel containing aluminum isopropylate and nickel nitrate. Nickel particles of the freshly prepared reduced catalysts were too small to calculate their size using X-ray diffraction data. In the catalyst after DRM, the size of nickel particles was 6 nm. All the catalysts had an ordered cylindrical mesoporous structure with an average pore diameter of 6–10 nm. The mesopore diameter of the material containing 10 wt % Ni decreased from 9.4 to 6.5 nm after reduction and remained almost unchanged after DRM. Catalysts with nickel loadings of 5, 7, and 10 wt % showed almost the same results in methane reforming. At 800°C , the methane and CO_2 conversions were about 90%. The catalyst with 10% Ni at 700°C remained stable for 100 h (reactants conversion of about 80%). Catalyst after 10 h on stream in DRM contained more carbon deposits than after 100 h. It is known that the Boudouard reaction barely proceeds at 700°C , and coking is due to methane pyrolysis. At the same time, carbon can be consumed in the periodic reactions $\text{C} + \text{CO}_2 \rightarrow 2\text{CO}$ and $\text{C} + \text{H}_2\text{O} \rightarrow \text{H}_2 + \text{CO}$, an assumption that is consistent with the cyclic change in the H_2/CO ratio observed in the 100-h run.

Newnham et al. [122] studied DRM catalysts similar to [121] in the synthesis procedure. Samples containing 7, 10 and 15 wt % nickel on mesoporous Al_2O_3 had the size of nickel clusters of 10, 11, and 19 nm and mesopore diameters of 14, 10, and 9 nm, respectively. Catalyst containing 10 wt % nickel showed stable values of methane conversion of 80%, CO_2 conversion of 90%, CO selectivity of 80%, and H_2 selectivity of 70% for 200 h at 800°C , at 900°C , the conversion of the reactants was close to 100%. It was noted that catalyst coking decreased with increasing DRM temperature.

An additional introduction of calcium ions into mesoporous $\text{NiO-Al}_2\text{O}_3$ catalysts diminished coking during the DRM process by more efficient binding of carbon dioxide to the catalyst surface [123].

In [124], a mesoporous alumina–nickel catalyst was doped with magnesium. The template synthesis method for the catalyst was similar to that described in [121–123]. The introduction of magnesium had almost no effect on the results of DRM in comparison with the mesoporous alumina–nickel catalyst without magnesium. Shen et al. [125] studied how the deposition of mesoporous silica on a nickel–aluminum complex oxide catalyst prepared from layered aluminum–magnesium double hydroxide affected the dry reforming of methane. After calcination and reduction, the

catalyst contained nickel particles of 8 to 9 nm size coated with mesoporous silica layer of 12–15 nm in thickness, as well as phases of the Ni–Mg–O solid solution and MgAl_2O_4 and NiAl_2O_4 spinels. The catalyst at 800°C showed stable values of methane and CO_2 conversion at the level of 90% for 8 h due to the resistance of nickel particles to aggregation, which leads to catalyst coking.

The oxide catalysts synthesized in [126] having a bimodal distribution of mesopores and containing Ni, Ce, Mg, and Al ions were obtained by adding sodium hydroxide to aqueous metal nitrate solutions, followed by prolonged boiling. The catalysts contained 5 wt % MgO and CeO_2 and variable amounts of nickel and aluminum oxides. Freshly prepared catalysts had narrow closed pores with a diameter of 4 nm and open pores with a diameter of 7–10 nm. A more active and stable catalyst initially contained 15 wt % nickel oxide. As a result of hydrogen reduction and use in DRM, the average pore diameter of the catalyst consistently increased from 8 to 9 and then to 14 nm. The size of nickel particles was 7 nm after reduction and increased to 9 nm after DRM. At 750°C , methane conversion of 97%, a CO_2 conversion of 80%, and CO and H_2 yields of 95 and 85% were achieved. An increase in the feed rate of the reactants worsened the results. An increase in the DRM temperature to 800°C did not affect the CO_2 conversion but increased the conversion of methane to 100%. During a 100-h test at 750°C , the conversion of methane and CO_2 decreased by 3%. In this case, a significant amount of carbon nanotubes (9 wt %) was formed, which could block the reactor. Various routes were distinguished for the formation of nickel particles. Calcination and reduction at $550\text{--}650^\circ\text{C}$ was accompanied by the reduction of nickel oxide to the metal, whereas similar procedures at 650°C were characterized by the formation and subsequent reduction of NiAl_2O_4 spinel, which led to the production of more stable nickel particles.

Zirconia-based DRM catalysts of the Ni–CaO– ZrO_2 composition were prepared by adding sodium hydroxide to aqueous solutions of nitrates of the elements to precipitate their hydroxides [127]. For the formation of mesopores, the precipitate was suspended with a solution of Pluronic P123 (a copolymer of polyethylene oxide and polypropylene oxide) as a structure-directing agent. After aging, the precipitate was washed to remove sodium ions and calcined to anneal the template. The catalyst reduced with hydrogen showed stable methane conversion of 77% and CO_2 conversion of 87% for 100 h of testing at 700°C at a feed rate of the undiluted reactants of $12 \text{ L}/(\text{g}_{\text{cat}} \text{ h})$. A decrease in temperature and an increase in the reactants feed rate led to rapid coking of the catalyst.

Zirconia with a mesopore diameter of 3–10 nm obtained using dodecylamine as the structure-directing agent, treated with ammonia, and loaded with 5 wt % nickel, catalyzed DRM at 750°C , showing

a methane conversion of 75 and 87% hydrogen selectivity [128]. The activity and selectivity of the catalyst were higher than those of an analogue based on zirconia obtained by simple precipitation.

Sokolov et al. [129] compared the activity of 5 wt % Ni/La₂O₃–ZrO₂ catalysts in DRM at 400°C. Nickel was deposited on supports of various structures: amorphous, mesoporous, and macroporous. The meso-structured catalyst, unlike the others, did not change activity for 180 h. The researchers believe that the cause of activity loss is not only coking, but also the formation of an oxide layer on the nickel surface, which is a very likely process at a low DRM temperature and low (less than 10%) syngas yields.

A number of publications that are not cited in this review can be found in [130]. In general, the material in this section shows the efficiency of stable meso-structured oxides of various natures as a support or matrix for nickel and nickel–cobalt particles catalyzing the POM and DRM reactions. The localization of active sites in mesopores and partly the possibility of their interaction with the support prevent the agglomeration of metal particles, thereby increasing the stability of the catalysts.

However, as shown in [131–133], preservation of the initial mesoporous structure is not compulsory for preparing active and stable POM and DRM catalysts. Mesoporous 5 wt % Ni(Co)–Gd_{0.1}Ti_{0.1}Zr_{0.1}Ce_{0.7}O₂ materials described in [131] were synthesized by coprecipitation of ions from aqueous nitrate solutions with potassium hydroxide. The mesoporous structure was formed using ultrasonic treatment. The materials washed to remove potassium ions and calcined at 500°C were characterized by narrow pore distribution with a diameter of 2–5 nm. After the catalysis of POM and DRM, a multimodal pore distribution with a diameter of 10 to 50 nm was observed. At the same time, the specific surface area decreased from 50–70 to 3–6 m²/g. In the POM reaction at 870–880°C on cobalt and mixed (2.5 wt %) nickel–cobalt contact catalysts, the yields of CO and hydrogen were 60%, wherein the nickel catalyst turned out to be less selective. However, the nickel catalyst showed better results in DRM. At 850°C, the yields of CO and hydrogen were 69 and 55%, respectively. In [132], it was found that in the optimal molar ratio in a mixed nickel–cobalt catalyst is Ni/Co = 8. The yields of CO and H₂ in POM were 88 and 84% at a temperature of 800°C and increased to 96 and 91%, respectively, at 850°C. The CO and hydrogen yields of 86 and 64%, respectively, were observed in DRM on the same catalyst at 840°C. An increase in the DRM temperature to 950°C led to an increase in the CO and hydrogen yields to 96 and 80%, respectively.

The catalyst that had shown the best results of POM and DRM in [132] was modified in [133] by partially replacing nickel and cobalt ions with manganese, iron, or copper ions. The amount of the modifier ion

was 10 or 20 wt % of the initial total content of nickel and cobalt ions. This amount did not lead to a noticeable change in the POM results, whereas the yields of CO and H₂ in the DRM reaction at 800°C were 80 and 84% due to the introduction of manganese, and they increased to 91% at 850°C. Long-term testing of this catalyst in POM for 60 h (920°C; CH₄/O₂ = 2; *W* = 9 L/(g_{cat} h)) [102] did not reveal a tendency to a decrease in the syngas yield. The diffraction pattern of the catalyst after POM exhibited intensive reflections of CeO₂, as well as trace amounts of MnO₂, Co₃O₄, and metallic nickel, cobalt, and manganese. After 60 h on stream, the catalyst was slightly coked.

Thus, the mesoporous structures of supported nickel and nickel–cobalt catalysts in some cases facilitate the selective and stable occurrence of POM and DRM reactions, mainly because of the prevention of agglomeration of nickel particles.

ZEOLITE-CONTAINING NICKEL, COBALT, AND NICKEL–COBALT POM AND DRM CATALYSTS

Natural and synthetic zeolites of various nature are crystalline aluminosilicates or metallosilicates, the framework of which is formed by [AlO₄] (or [MeO₄]) and [SiO₄] tetrahedra, making a system of micropores of various diameters. The presence of a microporous structure determines the molecular sieve effect of zeolites capable of selectively sorbing molecules of a certain size. The structure of aluminosilicate zeolites also contains ions of hydrogen or various metals, which compensate for the excess negative charge that is formed when silicon ions are replaced by aluminum in the crystal lattice. Zeolites are widely used as adsorbents. Due to the presence of Brønsted and Lewis acid sites, many zeolites are used in various catalytic processes. The high specific surface area of zeolites and the presence of a developed microporous structure suggest that these materials can also be used as supports for the formation of finely divided metal particles on their surface and in pores. Zeolites of the structural type MFI (trade name ZSM-5), which have high thermal stability and contain ordered pores of about 0.5 nm in size, are of particular interest for the preparation of POM and DRM catalysts. The use of zeolites of other types in POM and DRM is also reported.

To prepare DRM catalysts, Chang et al. [134] calcined a mixture of nickel nitrate or nickel, potassium, and calcium nitrates with ZSM-5 zeolite (Si/Al > 200) containing 20% alumina as binder. A nitrogen-diluted mixture of methane and CO₂ was fed into a reactor. The CO yield on the 5.3 wt % Ni/ZSM-5 catalyst at 700°C was 77%, with noticeable coke formation being observed. The addition of K and Ca ions slightly increased the yield of CO and eliminated coking. A decrease in the Ni loading of Ni/ZSM-5 to 2.4 wt % led to a decrease in the yield of CO to 70%, but also

suppressed coking. The increase in the Ni loading to 9.7 wt % increased the CO yield to 83%, but enhanced coking. Apparently, a decrease in the nickel loading prevents the formation of large nickel particles that facilitate coking. The KNiCa/ZSM-5 catalyst provided a quantitative yield of synthesis gas at 900°C. At 800°C, it showed a stable CO₂ conversion of 90–93% over 140 h, practically without coking.

Catalysts containing 5–7 wt % Ni on zeolite Y turned out to be more active in DRM than catalysts obtained by depositing Ni on zeolites A, X, and ZSM-5 [135]. At 800°C for 5 h, methane and CO₂ conversions remained stable at 92% with a hydrogen selectivity of 65%. The catalyst containing 3% Ni showed similar results at the beginning of the experiment, but its performance deteriorated over time. It should be noted that less active catalysts were less subjected to coking.

Catalytic activity in DRM at 600–640°C of nickel (1 wt %), platinum (0.5 wt %), and mixed nickel–platinum catalysts supported on dealuminated zeolites FAU, Y, and BEA was estimated as the number of moles of methane converted per gram of metal per hour [136]. The mixed nickel–platinum catalysts were less active than the platinum catalysts, whereas the nickel catalysts were inactive and were heavily coked. The best support was dealuminated zeolite BEA; the activity of NiPt/BEA was 1.9 mol/(g h) and that of Pt/BEA, 3.2 mol/(g h). The bimetallic Ni(2.5%)Rh(2.5%)/BEA catalyst [137] at 700°C showed methane and CO₂ conversion of 73 and 78%, respectively, which coincided with the results on 5% Rh/BEA. However, the rhodium catalyst did not undergo coking, whereas the bimetallic catalyst contained 3% coke after 2 h on stream. The 5% Ni/BEA catalyst showed close values for the initial conversion of the reactants, but it was quickly deactivated as a result of strong coking (7% coke after 2 h).

The addition of 0.1 wt % Rh to the 7.5% Ni/NaY DRM catalyst made it possible to achieve the 100% conversion of CO₂ and methane at 560–585°C [138]. The La₂NiO₄/ZSM-5 DRM catalyst [139] was obtained by immersing the zeolite in an aqueous solution containing nickel and lanthanum nitrates, citric acid, and ethylene glycol followed by evaporation and calcination. The dispersion of La₂NiO₄ spinel on the surface and in the pores of the zeolite was found to be uniform. The reduced catalyst contained nickel particles of a 13.5 nm size, which changed to 17.5 nm after DRM. According to X-ray diffraction data, the spinel decomposed to the oxides and the La₂O₂CO₃ phase was formed in the DRM process. The extremely low intensity of zeolite reflections in the X-ray diffraction patterns presented in the paper is surprising. The authors do not explain this fact. At 700°C, the conversions of CO₂ and CH₄ on La₂NiO₄/ZSM-5 remained at 70 and 65% for 36 h, with a selectivity of 95% for CO and 90% for H₂. The coke content periodically

changed from 0 to 5 wt %. The Ni/ZSM-5 and La₂NiO₄/γ-Al₂O₃ catalysts were significantly less active and stable and underwent coking.

By depositing 5–10 wt % Ni on BEA zeolite, a POM catalyst was obtained, which showed a quantitative yield of CO at 700–900°C [140]. The dealumination of the zeolite increases the stability of the catalyst, and a decrease in the nickel loading to 1 wt % significantly reduces its activity.

For the synthesis of Ni DRM catalysts, a silicate with a ferrierite (FER) zeolite structure, a silicalite with the MFI structure, and a silicate with the ordered mesoporous MCM-41 structure were used [141]. The Ni loading was 5 wt %. The catalysts showed comparable degrees of conversion of methane (63–77%) and CO₂ (83–90%) at 700°C; however, the best results were obtained on Ni/FER, stable for 30 h.

Nickel, cobalt, and mixed nickel–cobalt catalysts deposited by impregnation onto ZSM-5 zeolite (Si/Al = 11.5) were also studied in dry reforming of methane [142]. The metal loading of the catalysts was 7 wt %. Close values of hydrogen yield, 58–65%, were observed in the range of 600–800°C on the catalysts, with the exception of the cobalt-loaded one. On the cobalt catalyst, such a hydrogen yield was reached only above 700°C. At the same time, this catalyst was most selective for CO at 600°C (68%). At 800°C, the CO selectivity of all the catalysts was approximately the same, 60–62%. The nickel catalyst was prone to coking, being inferior to the mixed nickel–cobalt contact catalysts in the conversion of methane and CO₂. In general, a catalyst with a ratio of Ni/Co = 0.5 turned out to be more active and stable. The conversion of CO₂ at 800°C was 85%; that of methane, 75%; the syngas selectivity was 63%; and the degree of coking was less than 1%.

Ultrasonic treatment of a catalyst containing cobalt supported on zeolite H-Y made it possible to obtain more active DRM catalysts by increasing the dispersion of cobalt particles [143]. The catalyst with a cobalt loading of 10 wt % ensured hydrogen and CO yields of 61 and 80%, respectively, at 850°C or 55 and 77% at 750°C. However, conversion of methane and CO₂ on the catalyst markedly decreased after 10 h on stream.

Nickel–platinum catalysts supported on a silicalite of the MFI structure and encapsulated in a silicate shell were tested in the DRM reaction [144]. Catalyst containing 1.5 wt % Ni and 0.5 wt % Pt showed methane and CO₂ conversion of about 80% at 800°C; however, these values decreased to 60% after 20 h on stream. The platinum-free catalyst deactivated much faster. The catalysts that had not been encapsulated in SiO₂ completely lost their activity after 1–6 h.

The results of DRM depend on the Si/Al ratio in Ni catalysts supported on NaZSM-5 zeolite [145]. At 800°C, the best performance was obtained on the catalyst with a Ni loading of 5 wt % and Si/Al = 30: CO₂

conversion, 98%, CH₄ conversion, 95%; H₂/CO ratio, 0.91. The catalyst operated stably for 30 h. The amount of coke deposits did not exceed 1 wt %. At a higher silica ratio, the results worsened, with the silicon-free 5% Ni/ γ -Al₂O₃ catalyst being the most active in DRM, although its stability was not examined.

10% Ni/25% CeO₂-ZrO₂/ZSM-5 catalyst, prepared by depositing nickel from a nitrate solution on a ceria-zirconia mixture with the zeolite and subsequent sonicating, showed activity in POM already at 400°C, providing a 50% methane conversion and a CO yield of 10%. At 700°C, methane conversion reaches 90% [146]. These characteristics remained unchanged for 25 h. The zeolite-free Ni/CeO₂-ZrO₂ catalyst quickly deactivated at 700°C after 4 h of POM.

Catalysts with a variable amount of Ni and Co supported on zeolite Y in the H form (Si/Al = 2) from aqueous nitrate solutions under ultrasonic treatment were used for DRM in [147]. The maximum H₂ and CO yields of 92 and 98%, respectively, were obtained on the 7%-Ni3% Co/Y catalyst at 850°C and a reactants (CH₄/CO₂ = 1) feed rate of 24 L/(g_{cat} h). The catalyst remained stable in DRM for 10 h.

In [148], the POM and DRM reactions were studied using nickel, cobalt, and nickel-cobalt catalysts deposited by impregnation on H-form MFI zeolites synthesized by various methods. A commercial sample with Si/Al = 38 and 20 wt % alumina binder contained zeolite synthesized by the conventional hydrothermal method (denoted by MFIht). Another zeolite MFI_{mw} (Si/Al = 20), synthesized with the use of microwave radiation as described in [149], was binder-free. The catalysts contained 2 wt % nickel or cobalt or both in an amount of 1 wt % each. The POM and DRM reactions were carried out without preliminary reduction of the catalysts. In the POM reaction at 800°C, methane conversion values of 95 and 93%, CO yields of 92 and 89%, and H₂ yields of 92 and 86% were observed on the NiMFI_{mw} and NiCoMFI_{mw} catalysts, respectively. With an increase in temperature to 900°C, methane conversion on NiMFI and NiCoMFI catalysts increased to 97 and 98%, respectively, and the yields of CO and H₂ increased to 97%. CoMFI_{mw} was inactive throughout the entire temperature range. The unreduced NiMFIht and NiCoMFIht catalysts showed activity in POM only when they were heated in a methane-oxygen mixture to 900–920°C. The most active catalyst was NiCoMFIht, which showed a methane conversion of 70%, a CO yield of 65%, and an H₂ yield of 60% at 920°C.

In the DRM reaction at 800°C on the NiMFI_{mw} or the NiCoMFI_{mw} catalyst, methane conversion of 73 or 88%, CO₂ conversion of 80 or 90%, CO yield of 76 or 88%, and H₂ yield of 58 or 72%, respectively, were observed. With increasing temperature, the results of DRM improved, with the mixed nickel-

cobalt catalyst being more active and selective. At 920°C, the yields of CO and H₂ reached 97%.

NiMFIht and NiCoMFIht, which are based on the commercial zeolite with the binder and exhibit low activity in POM, proved to be much better in DRM. Upon reaching 800°C, the NiMFIht and NiCoMFIht catalysts showed degrees of methane conversion of 81 and 90%, CO₂ conversions of 81 and 92%, CO yields of 80 and 89%, and H₂ yields of 81 and 76%, respectively. The results improved with increasing temperature, but the mixed nickel-cobalt catalyst also remained more active and selective. At 900°C, the yields of CO and H₂ reached 97 and 91%, respectively, but the hydrogen yield decreased at higher temperatures as a result of hydrogenation of CO₂ to CO.

In general, the mixed nickel-cobalt catalyst based on MFI zeolite synthesized using microwave treatment effectively catalyzed POM and DRM without suffering from coking. The analogues terpart based on the commercial zeolite with the binder was effective only in the catalysis of DRM, but carbon nanotubes are visible in its micrographs after DRM. It should be noted that all the catalysts studied in [148] retained the MFI structure intact after carrying out catalytic experiments.

In [102], we studied the stability in the POM and DRM processes for the nickel-cobalt catalyst described in [148], which was supported on the MFI zeolite prepared by microwave-assisted synthesis. Testing of the catalyst in the cyclic POM process revealed its on-stream instability. The freshly prepared catalyst heated to 900°C in a flow of CH₄/O₂ = 2 at a feed rate of 12 L/(g_{cat} h) operated stably for 5.5 h, showing CO yields of 95–99% and H₂ yields of 90%. However, after cooling and reheating in a methane-oxygen mixture, the catalyst turned out to be completely inactive in POM. An increase in the total Ni and Co (1 : 1) loading from 2 to 8% led to similar results. At the same time, the 1% Ni1% CoMFI_{mw} catalyst heated to 900°C in a stream of CH₄/CO₂ = 1, fed at a rate of 15 L/(g_{cat} h), stably catalyzed the DRM reaction for 31 h in a cyclic mode. The yields of CO and H₂ were 90%. The 8% Ni8% Co/MFI_{mw} catalyst showed stable CO and H₂ yields of 96–97% for 70 h. The diffraction patterns of the catalysts after DRM exhibited intensive reflections of MFI zeolite, less intense reflections of Ni and Co metal particles, and the absence of noticeable amounts of nickel and cobalt oxides. Thus, an effective approach to the design of active and stable nickel and nickel-cobalt catalysts for DRM reaction is the introduction of these metals into the matrix of microporous zeolites. The resulting catalysts are superior to the alumina-supported. The data on the use of zeolite based catalysts in POM are controversial.

NICKEL, COBALT, AND NICKEL-COBALT
POM AND DRM CATALYSTS BASED
ON ALUMINUM-MAGNESIUM
HYDROXIDES OF HYDROTALCITE
STRUCTURE

In the aforementioned study [125], the effect of the deposition of mesoporous silica onto a nickel–aluminum–magnesium complex oxide catalyst, prepared from a layered aluminum–magnesium double hydroxide of a hydrotalcite structure, on the DRM process was investigated. The on-stream stability of the catalyst at 800°C for 8 h (methane and CO₂ conversion of 90%) was attributed to the formation (after calcination and reduction) of 8–9 nm nickel particles, Ni–Mg–O solid solution, and MgAl₂O₄ and NiAl₂O₄ spinels.

According to [1–10], the formation of the NiAl₂O₄ spinel is one of the reasons for the deactivation of Ni/Al₂O₃ POM catalysts. At the same time, as shown in [126], it is via the formation and subsequent reduction of NiAl₂O₄ spinel leading to the production of more stable nickel particles that oxide catalysts having a bimodal distribution of mesopores and containing Ni, Ce, Mg, and Al ions generated DRM active sites. Numerous published data also show that the presence of magnesium oxide in the catalysts generally have a positive effect on the course of POM and DRM [1–10].

Extensive studies of nickel catalysts in the aluminum–magnesium oxide matrix were carried out with the aim of creating coke-resistant DRM catalysts. Thus, MgAl₂O₄ spinel, the formation of which often occurs during catalysis by nickel–MgAl–hydrotalcite systems, was used as a support for a nickel catalyst [150]. The 16% Ni/MgAl₂O₄ catalyst prerduced with hydrogen at 550°C was more active in DRM than catalysts containing 1–2 wt % platinum metals supported on aluminum-stabilized magnesium oxide. No data on conversion and selectivity was given in the cited paper, limited to reporting the catalyst turnover number.

A catalyst with an atomic ratio of Ni/Mg/Al = 10/61/29 (which corresponds to Ni content of 15 wt %) at 800°C and short contact times ensures the complete conversion of oxygen in a helium-diluted methane–oxygen mixture and a methane conversion, as well as selectivity for CO and H₂, of more than 90% [151]. Significant catalyst coking is due to the formation of large nickel particles, on which the following reactions can occur: CH₄ → C + 2H₂; 2CO → C + CO₂, while POM mainly proceeds on small nickel particles (on the order of 12 nm, which are not displayed on the diffraction patterns). In experiments on POM with short contact times, a higher temperature was recorded at the end of the catalyst bed, which is inconsistent with the generally accepted POM mechanism, the initial step of which is the combustion of

methane to give CO₂ and H₂O, which then react with an excess of methane to form synthesis gas.

The data presented show the effectiveness of the approach to the formation of DRM and POM catalysts by dispersing nickel and cobalt ions in an aluminum–magnesium oxide matrix. A comparatively new approach to the design of such catalysts is the dispersion of nickel and cobalt ions in the structure of layered aluminum–magnesium hydroxides of a hydrotalcite structure, accompanied by partial replacement of magnesium ions in the structure of the materials.

Hydrotalcite-derived nickel catalysts for CO₂/steam reforming have been patented [152]. The catalysts were reduced with hydrogen at 850°C and 20 atm and tested in carbon dioxide reforming of methane at 800–900°C, 7–20 atm, and a four-fold molar excess of CO₂ with various amounts of feed steam. The catalysts with a variable ratio of Ni, Al, and Mg at 850°C and 7 atm showed close methane and CO₂ conversions of 92–96 and 54–69%, respectively. The absence of noticeable coking was reported. No data on DRM results is given in [152].

Shishido et al. [153] studied the use of aluminum magnesium hydrotalcites, to which nickel was introduced by coprecipitation or impregnation, as precursors of DRM catalysts. Catalysts containing 25 wt % nickel were formed after calcination. A nitrogen-diluted mixture of methane and CO₂ was fed to the reactor. The catalysts obtained by either coprecipitation or impregnation did not mediate methane conversion at temperatures below 750°C, whereas the conversion sharply increased to 80% when this temperature was reached. At 800°C, the methane conversion was as high as 94%, being stable for 6. The catalyst obtained by coprecipitation formed more coke per unit mass of the catalyst, but a smaller amount per unit surface. According to the XRD data, the spent catalysts contained phases of metallic nickel, magnesium and nickel oxides, and aluminum–magnesium spinel.

The results of POM at 600–800°C depend on the Mg/Al ratio in a hydrotalcite-based catalyst containing 20 wt % Ni [154]. The catalysts were previously reduced in a stream of hydrogen. After POM, the hydrotalcite phase was absent and the phases of MgO, NiO, NiAl₂O₄, and metallic Ni were present in the samples. The presence of NiAl₂O₄ makes it difficult to reduce NiO to the metal. The catalyst obtained on the basis of the sample with Mg/Al = 4.85, which had the highest degree of crystallinity, showed better results and higher coke resistance due to both the small size of the formed nickel particles and the presence of NiAl₂O₄ spinel, which prevents methane dissociation. Above 700°C, the complete oxygen conversion was achieved, and methane conversion and selectivity for H₂ and CO reached 97, 95, and 94%, respectively, at 800°C.

Tsyganok et al. [155] collated the catalytic properties in the DRM for Ni–Al–Mg hydrotalcite catalysts obtained by the conventional coprecipitation technique and catalysts into which nickel ions were introduced in the form of ethylenediaminetetraacetate (EDTA) complexes. In the latter case, instead of isomorphous substitution for magnesium ions in the hydrotalcite structure, nickel ions were located between layers in the layered structure of the hydrotalcite matrix. The catalysts were reduced in a nitrogen–hydrogen mixture at 600°C and, after cooling in a stream of nitrogen, heated to 800°C in a methane–nitrogen–carbon dioxide stream. Conversion and selectivity values close to 100% were observed for a NiMg₁₁Al_{3.3}O₁₇ sample, into which nickel was introduced by ion exchange of MgAlNO₃ hydrotalcite with [NiEDTA]²⁻, and a NiMg₁₁Al₃O_{16.5} sample obtained by treating calcined MgAl hydrotalcite with an aqueous [NiEDTA]²⁻ solution. The catalysts contained approximately 9 wt % nickel. They were somewhat superior to the catalyst obtained by coprecipitation of magnesium and aluminum ions from their salts and nickel from [NiEDTA]²⁻. The composition of this material after calcination—NiMg₇Al₂O₁₁—corresponded to a nickel content of 13 wt %. The advantage of this catalyst was higher resistance to coking (5 wt % after 6 h) relative to more active catalysts containing 13–15 wt % carbon after 6 h on stream. The more coke-resistant catalyst contained 16-nm nickel particles, and the others had a particle size of 23–24 nm.

The Ni_{0.5}/Mg_{2.5}Al catalyst prepared from a hydrotalcite-like material and containing 16.3% Ni [156] was no worse than 1% Rh/MgO in terms of methane conversion in the POM process. Nickel particles of a 6–7 nm size formed in the reduced catalyst provided reaching a methane conversion of 93% at 800°C. No data on selectivity were reported in the cited paper. Before the POM experiments, the reduced catalyst contained the phases of MgAl₂O₄, MgO(NiO), solid solution, and metallic Ni.

The results of DRM using MgAl₂O₄ spinel catalysts varied depending on the nickel content in the range from 1 to 15 wt % [157]. After reducing the catalyst with hydrogen at 750°C, an undiluted mixture of methane and CO₂ was fed into the reactor at the same temperature. The methane and CO₂ conversions increased from 72 to 84% and from 85 to 94%, respectively, with an increase in the nickel content from 1 to 15%. At the same time, the catalyst stability increased as monitored over 10 h. An increase in the amount of coke from 1.5 to 39 wt % was also noted. On the 5 wt % Ni/MgAl₂O₄ catalyst, the methane and CO₂ conversions remained stable at 83 and 87%, respectively, for 55 h; the CO and H₂ selectivities varied in the range of 97–99%, and coking made 4.6 wt %. In addition to MgAl₂O₄ reflections, X-ray diffraction patterns of the

catalyst after DRM displayed reflections of metallic nickel with a particle size of 10–12 nm.

DRM catalysts containing Ni, Mg, and Al oxides as obtained from a hydrotalcite-like precursor synthesized by coprecipitation with a sodium carbonate solution had a mesoporous structure with a pore diameter of 4–19 nm [158]. Depending on the Mg/Al ratio, their specific surface area varied from 145 to 220 m²/g. The amount of nickel was 10% of the total magnesium and aluminum oxides (9% of catalyst weight). The catalyst was reduced in a stream of hydrogen at 800°C, and an undiluted equimolar mixture of methane and CO₂ was fed. An increase in the Mg/Al ratio from 0.25 to 4 led to a decrease in the size of nickel particles in the catalysts after DRM from 19 to 11 nm. When the size of nickel particles was less than 15 nm, the coking of the catalyst ceased. The methane and CO₂ conversions remained almost unchanged with a change in the Mg/Al ratio and amounted to 81–86 and 84–87%, respectively.

Perez-Lopez et al. [159] studied DRM in the presence of catalysts similar to those described in [158], but containing >25 wt % Ni. The catalyst was reduced with a nitrogen–hydrogen mixture at 700°C. Then, a nitrogen-diluted 1 : 2 methane–carbon dioxide mixture was fed with increasing the temperature from 500 to 700°C. As the temperature was increased to 700°C, the methane conversion reached 90–93% and the CO₂ conversion did not exceed 50%. The more active catalyst contained 5-nm nickel particles. It was found that the use of catalysts with molar ratios of 5 > Ni/Mg > 1, Mg/Al > 1/3, and M^{II}/M^{III} = 2 is preferable.

The POM catalysts, obtained by coprecipitation of magnesium and aluminum oxides, with Mg/Al ratios of 0.25 and 0.5 and a Ni loading of 5 wt % [160] showed methane conversion and CO selectivity close to 100% at 900°C. The hydrogen selectivity was about 90%. A gas mixture strongly diluted with helium was fed to the reactor, and the catalyst was tested with a gradual increase in temperature without preliminary reduction. The formation of synthesis gas began after heating to 800°C. During 72 h of testing, a decrease in methane conversion to 90% and hydrogen selectivity to 80% was observed. Adding gold in an amount of 5 wt % to the catalyst stabilized high methane conversion and CO selectivity, reduced coking, but did not affect hydrogen selectivity. After reduction of freshly prepared catalysts in a stream of hydrogen at 900°C, the phases of metallic Ni and MgAl₂O₄ or NiAl₂O₄ were detected on the X-ray diffraction pattern of the sample with Mg/Al = 0.25 and no reflections due to crystallized MgO were found. At an Mg/Al ratio of 0.5, only wide low-intensity reflections of MgAl₂O₄ or NiAl₂O₄ were observed. The addition of gold to the catalysts sharply increased the intensity of the reflections and led to the appearance of the MgO reflection. Gold, according to the authors, was present in the form of an alloy with nickel.

Lanthanum-promoted NiMgAl oxide DRM catalysts derived from hydrotalcite-like precursors were studied in [161–164]. Comparison of the properties of catalysts containing 2 wt % Ni and from 0 to 2 wt % La showed a decrease in activity and an increase in stability in DRM with an increase in the lanthanum content [161]. The experiments were carried out at 750°C and a low conversion of the reactants (less than 50%).

An increase in the Mg/Al molar ratio decreased the activity, but the stability of the catalysts increased [162]. On a catalyst with an atomic ratio of Mg/Al = 2.3, containing 2.8 wt % nickel and 1.9 wt % lanthanum, the CO₂ conversion at 750°C for 300 h retained a stable value of about 92% and the methane conversion was lower by 2 to 3%. The formation of carbon nanotubes and nanofibers was noted. The rate of coking was 2 mg/(g_{cat} h) [163, 164].

In [165], DRM catalysts obtained by coprecipitation of Co, Al, and Mg nitrates with sodium carbonate were studied; after calcination, they contained from 34 to 53 wt % cobalt. According to X-ray powder diffraction data, the phases of Co₃O₄ and CoAl₂O₄ were hardly distinguishable. In contrast to the data on the low performance of cobalt catalysts in DRM [1–3], the obtained catalysts after reduction with a hydrogen–nitrogen mixture made it possible to achieve a methane conversion of 65% at a relatively low temperature of 550°C. De Souza et al. [165] attribute the results to the promoting effect of magnesium and the presence of a significant amount of Co₃O₄, which is easier to reduce to metallic cobalt than CoAl₂O₄. The disadvantage of the catalysts is the significant formation of carbon fibers.

The use of mixed Ni–Co–Mg–Al oxides obtained from precursors of a layered hydrotalcite structure (synthesized by coprecipitation from nitrate solutions) in DRM was studied in [166]. The composition of the catalysts after calcination is described by the general formula Co_xNi_yMg_zAl₂, where x and $y = 0, 1, 2, 3, \text{ or } 4$; $z = 2 \text{ or } 4$; and $x + y + z = 6$. This formula corresponds to an approximate cobalt and/or nickel content of 29 or 49 wt %, respectively. The catalysts were preconditioned for 2 h in a hydrogen–argon flow at 800°C and cooled in argon to 400°C, after which an argon-diluted equimolar mixture of methane and CO₂ was fed into the reactor. The temperature in the reactor was gradually raised to 800°C. Over the entire temperature range, no significant differences were observed in the values of CO₂ conversion achieved on catalysts of various compositions and with different nickel and cobalt contents. Below 700°C, the methane conversion on the cobalt-rich catalysts Co₂Mg₄Al₂ and Co₃NiMg₂Al₂ was noticeably lower. The same catalysts were more resistant to coking. At 800°C, the methane and CO₂ conversions increased to 93–98%. In this case, the yield of hydrogen reached 65% and the yield of CO, 75%. Despite the close yields of the

desired products, the Co₂Ni₂Mg₂Al₂ sample containing the equivalent amount of nickel and cobalt, a total of 49 wt %, was the most effective according to the authors of the cited paper. By the XRD method, phases of carbon, metallic nickel and cobalt, magnesium oxide, and nickel–cobalt and nickel–aluminum carbides were detected in the spent catalysts.

All the catalysts described above contain a significant amount of nickel and/or cobalt and are generally not free of coking. Aluminum–magnesium hydrotalcite-based DRM catalysts containing less than 5 wt % nickel showed methane and CO₂ conversions of less than 90% with noticeable coking [157], or being additionally promoted with lanthanum, could provide methane and CO₂ conversion values of about 90%, but did not eliminate the formation of carbon nanofibers and nanotubes [163, 164].

The catalysts developed in [167] based on hydroxo salts of the general formula [AlMg₂Ni_xCo_y(OH)_{6.08}][(NO₃)_nH₂O], where $x = 0, 0.02, \text{ or } 0.04$ and $y = 0, 0.02, \text{ or } 0.04$, with hydrotalcite-like structure, contain Ni and/or Co in an amount of no more than 2 wt % in total. It has been shown that the Ni-containing catalysts make it possible to achieve a 90% syngas yield in POM and 97% in DRM. Only an insignificant amount of carbon nanotubes is formed. Simultaneous Ni and Co presence makes a catalyst not to form carbon nanotubes at all during dry methane reforming.

Testing these catalysts for stability showed [102] that after short-term heating to 950°C in a stream of methane–oxygen mixture (CH₄/O₂ = 2; feed rate of 12 L/(g_{cat} h)), the aluminum–magnesium hydrotalcite-derived catalyst containing 2 wt % Ni continues to work stably in the POM reaction at 900°C for 50 h, demonstrating a high (over 90%) yield of synthesis gas. Micrographs of the catalyst after POM showed no signs of catalyst coking.

The same catalyst in the DRM reaction stably operated for 60 h, showing a high (more than 95%) syngas yield. Microphotographs of the catalyst surface after DRM showed fragmentary accumulations of particles of nickel or its oxide, as well as minor carbon deposits associated with them, which apparently do not affect the stability of the catalyst in DRM. The X-ray diffraction patterns of the catalyst after POM and DRM were identical and allowed the detection of only MgO and spinel phases containing magnesium or nickel and cobalt along with aluminum. A likely reason for the stability of the catalyst in POM and DRM is the small size of the nickel particles formed, which do not give reflections on X-ray diffraction patterns. This finding is consistent with the data obtained by Shishido et al. [153], who studied DRM on aluminum–magnesium hydrotalcite catalysts containing 10% nickel. They found that when the size of nickel particles is less than 15 nm, catalyst coking stops.

The analysis of the literature data presented in this section shows that catalysts containing nickel and cobalt dispersed in an aluminum–magnesium hydroxide matrix hold promise for use in the POM and DRM processes. The activity, selectivity, and stability of the catalysts are usually associated with the formation of nickel nanoparticles and the presence of magnesium oxide and magnesium–aluminum spinel. The addition of cobalt reduces the coking of catalysts in some cases. Aluminum–magnesium hydroxide proved to be the preferred support for preparing of a 2% nickel catalyst, which provides a stably high yield of synthesis gas in the processes of both partial oxidation and dry reforming of methane [102]. This catalyst can be considered promising for the practical implementation of the POM and DRM processes.

CONCLUSIONS

The analysis of the cited material shows that the formation of stable nanosized (less than 15 nm) particles of metallic nickel is a key approach to the creation of active, selective, and stable nickel, cobalt, and nickel–cobalt catalysts for partial oxidation and dry reforming of methane. The particles of this size preclude the intensive coking of the catalysts and, in some cases, promote the oxidation of the carbon particles formed. Stable nanosized nickel particles can be formed by means of all the methods discussed in the review:

—the use of REE-containing perovskite and perovskite-like complex oxide systems as catalyst precursors;

—dispersion of nickel particles in a mesoporous or microporous (zeolite) matrix;

—the formation of nickel-containing catalysts based on preliminarily synthesized nickel-containing aluminum–magnesium hydroxides of hydroxide structure;

—doping of nickel catalysts with optimal amounts of rare earth elements and/or cobalt.

Each of these approaches makes it possible to obtain catalysts for the partial oxidation and dry reforming of methane into synthesis gas, which ensure comparable high yields of synthesis gas and high stability during long-term tests. The final selection of promising catalytic systems for the implementation of these processes requires pilot testing on a large scale.

FIUNDING

This work was supported by the Ministry of Education and Science of Russia (state assignment “Leading Researchers on an Ongoing Basis”, project no. 4.6718.2017/LS, questionnaire no. FSZE-2017-0008) and the Presidium of the Russian Academy of Sciences under program no. 14 “Physical chemistry of adsorption phenomena and actinide nanoparticles.”

CONFLICT OF INTEREST

The authors declare that there is no conflict of interest requiring disclosure in this article.

REFERENCES

1. A. Holmen, *Catal. Today* **142**, 2 (2009).
2. *Hydrogen and Syngas Production and Purification Technologies*, Ed. by K. Liu, C. Song, and V. Subramani (Wiley, Hoboken, NJ, 2009).
3. V. S. Arutyunov and O. V. Krylov, *Oxidative Conversion of Methane* (Nauka, Moscow, 1998) [in Russian].
4. O. V. Krylov, *Heterogeneous Catalysis* (Akademkniga, Moscow, 2004) [in Russian].
5. V. S. Arutyunov and O. V. Krylov, *Usp. Khim.* **74**, 1216 (2005).
6. N. Ya. Usachev, V. V. Kharlamov, E. P. Belanova, et al., *Russ. Chem. Rev.* **52** (4), 22 (2008).
7. N. Ya. Usachev, V. V. Kharlamov, E. P. Belanova, et al., *Pet. Chem.* **51**, 96 (2011).
8. Y. H. Hu and E. Ruckenstein, *Adv. Catal.* **48**, 297 (2004).
9. B. C. Enger, R. Lodeng, and A. Holmen, *Appl. Catal., A* **346**, 1 (2008).
10. B. C. Enger, R. Lodeng, and A. Holmen, *Catal. Lett.* **134**, 13 (2010).
11. A. G. Dedov, A. S. Loktev, D. A. Komissarenko, et al., *Appl. Catal., A* **489**, 140 (2015).
12. B. Zhenghong and Y. Fei, *Adv. Bioenergy* **3**, 43 (2018).
13. J. S. Kang, D. H. Kim, S. D. Lee, et al., *Appl. Catal., A* **332**, 153 (2007).
14. C. S. Song and P. Wei, *Catal. Today* **98**, 463 (2004).
15. M. A. Pena, J. P. Gomez, and J. L. G. Fierro, *Appl. Catal., A* **144**, 7 (1996).
16. S. A. Al-Sayari, *Open Catal. J.* **6**, 17 (2013).
17. H. Liander, *Trans. Faraday Soc.* **25**, 462 (1929).
18. K. Dossunov, G. Y. Yergazyieva, L. K. Myltykbayeva, et al., *Coke Chem.* **58**, 178 (2015).
19. Y. Ji, W. Li, H. Xu, and Y. Chen, *Appl. Catal., A* **213**, 25 (2001).
20. H. M. Swaan, R. Rouanet, P. Widyananda, and C. Mirodatos, *Stud. Surf. Sci. Catal.* **107**, 447 (1997).
21. C. T. Au, Y. H. Hu, and H. L. Wan, *Catal. Lett.* **11**, 199 (1994).
22. H. Y. Wang and E. Ruckenstein, *Catal. Lett.* **75**, 13 (2001).
23. V. R. Choudhary, S. D. Sansare, and A. S. Mamman, *Appl. Catal., A* **90**, 1 (1992).
24. Y. H. Hu and E. Ruckenstein, *Catal. Lett.* **57**, 167 (1999).
25. H. Y. Wang and E. Ruckenstein, *J. Catal.* **199**, 309 (2001).
26. V. R. Choudhary, V. H. Rane, and A. M. Rajput, *Catal. Lett.* **22**, 289 (1993).
27. X. Bi, P. Hong, X. Xie, and S. Dai, *React. Kinet. Catal. Lett.* **66**, 381 (1999).
28. L. D. Vella, J. A. Villoria, S. Specchia, et al., *Catal. Today* **171**, 84 (2011).

29. W. Dong, K. Jun, H. Roh, et al., *Catal. Lett.* **78**, 215 (2002).
30. H. Liu and D. He, *Catal. Surv. Asia* **16**, 53 (2012).
31. G. Pantaleoa, V. La Parola, F. Deganello, et al., *Appl. Catal., B* **189**, 233 (2016).
32. R. K. Singha, A. Shukla, A. Yadav, et al., *Appl. Catal., B* **202**, 473 (2017).
33. A. G. Bhavani, W. Y. Kim, J. W. Lee, and J. S. Lee, *ChemCatChem* **7**, 1445 (2015).
34. J. Cihlar, Jr., R. Vrba, K. Castkova, and J. Cihlar, *Int. J. Hydrogen Energy* **42**, 19920 (2017).
35. R. Jin, Y. Chen, W. Li, et al., *Appl. Catal., A* **201**, 71 (2000).
36. L. Rodrigues, R. B. Silva, M. G. C. Rocha, et al., *Catal. Today* **197**, 137 (2012).
37. C. T. Au, Y. H. Hu, and H. L. Wan, *Catal. Lett.* **11**, 199 (1994).
38. M. Li and A. C. van Veen, *Appl. Catal., B* **237**, 641 (2018).
39. T. H. Nguyen, A. Lamacz, P. Beaunier, et al., *Appl. Catal., B* **152–153**, 360 (2014).
40. T. H. Nguyen, A. Lamacz, A. Krzton, et al., *Appl. Catal., B* **165**, 389 (2015).
41. T. H. Nguyen, A. Lamacz, A. Krzton, et al., *Appl. Catal., B* **182**, 385 (2016).
42. T. H. Nguyen, A. Lamacz, A. Krzton, and G. Djega-Mariadassou, *Appl. Catal., B* **199**, 424 (2016).
43. V. A. Kondratenko, C. Berger-Karin, and E. V. Kondratenko, *ACS Catal.* **4**, 3136 (2014).
44. J. B. Claridge, M. L. H. Green, S. C. Tsang, et al., *Catal. Lett.* **22**, 299 (1993).
45. M. C. J. Bradford and M. A. Vannice, *Appl. Catal., A* **142**, 73 (1996).
46. M. C. J. Bradford and M. A. Vannice, *Catal. Rev. Sci. Eng.* **41**, 1 (1999).
47. A. P. E. York, T. Xiao, M. L. H. Green, and J. B. Claridge, *Catal. Rev. Sci. Eng.* **49**, 511 (2007).
48. V. Yu. Bychkov, O. V. Krylov, and V. N. Korchak, *Kinet. Catal.* **43**, 86 (2002).
49. V. Yu. Bychkov, Yu. P. Tyulenin, O. V. Krylov, and V. N. Korchak, *Kinet. Catal.* **43**, 724 (2002).
50. V. Yu. Bychkov, Yu. P. Tyulenin, and V. N. Korchak, *Kinet. Catal.* **44**, 353 (2003).
51. W. Shan, M. Fleys, F. Lopicque, et al., *Appl. Catal., A* **311**, 24 (2006).
52. A. Garcia, N. Becerra, L. Garcia, et al., *Adv. Chem. Eng. Sci.* **1**, 169 (2011).
53. X. Yin and L. Hong, *Appl. Catal., A* **371**, 153 (2009).
54. V. R. Choudhary, K. C. Mondal, A. S. Mamman, and U. A. Joshi, *Catal. Lett.* **100**, 271 (2005).
55. C. R. B. Silva, L. da Conceição, N. F. P. Ribeiro, and M. M. V. M. Souza, *Catal. Commun.* **12**, 665 (2011).
56. M. Morales, F. Espiell, and M. Segarra, *Int. J. Hydrogen Energy* **39**, 6454 (2014).
57. C. Guo, X. Zhang, J. Zhang, and Y. Wang, *J. Mol. Catal., A* **269**, 254 (2007).
58. M. A. Pena and J. L. G. Fierro, *Chem. Rev.* **101**, 1981 (2001).
59. S. Royer, D. Duprez, F. Can, et al., *Chem. Rev.* **114**, 10292 (2014).
60. F. Mudu, U. Olsbye, B. Arstad, et al., *Appl. Catal., A* **523**, 171 (2016).
61. A. Thursfield, A. Murugan, R. Franca, and I. S. Metcalfe, *Energy Environ. Sci.* **5**, 7421 (2012).
62. M. Stojanovic, C. A. Mims, H. Moudallal, et al., *J. Catal.* **166**, 324 (1997).
63. M. Crespin and W. K. Halls, *J. Catal.* **69**, 359 (1981).
64. H. Zhu, P. Zhang, and S. Dai, *ACS Catal.* **5**, 6370 (2015).
65. J. Cheng and A. Navrotsky, *J. Mater. Res.* **18**, 2501 (2003).
66. J. Staniforth, S. E. Evans, O. J. Good, et al., *Dalton Trans.* **43**, 15022 (2014).
67. H. Provendier, C. Petit, C. Estournes, et al., *Appl. Catal., A* **180**, 163 (1999).
68. K. T. C. Roseno, R. Brackmann, M. A. Silva, and M. Schmal, *Int. J. Hydrogen Energy* **41**, 18178 (2016).
69. G. C. de Araujo, S. Lima, M. C. Rangel, et al., *Catal. Today* **107–108**, 906 (2005).
70. J. Cheng and A. Navrotsky, *J. Mater. Res.* **20**, 191 (2005).
71. R. Lago, G. Bini, M. A. Pena, and J. L. G. Fierro, *J. Catal.* **167**, 198 (1997).
72. T. Hayakawa, H. Harihara, A. G. Andersen, et al., *Appl. Catal., A* **149**, 391 (1997).
73. A. Slagtern and U. Olsbye, *Appl. Catal., A* **110**, 99 (1994).
74. F. S. Toniolo, R. N. Magalhaes, C. A. Perez, and M. Schmal, *Appl. Catal., A* **117–118**, 156 (2012).
75. H. Provendier, C. Petit, C. Estoumes, and A. Kiennemann, *Stud. Surf. Sci. Catal.* **119**, 741 (1998).
76. K. Y. Pradeep and D. Taraknath, *Int. J. Hydrogen Energy* **44**, 1659 (2019).
77. J. W. Nam, H. Chae, S. H. Lee, et al., *Stud. Surf. Sci. Catal.* **119**, 843 (1998).
78. M. S. Santos, R. C. R. Neto, F. B. Noronha, et al., *Catal. Today* **299**, 229 (2018).
79. W.-J. Jang, J.-O. Shim, H.-M. Kim, et al., *Catal. Today* **324**, 15 (2019).
80. C. Batiot-Dupeyrat, G. Valderrama, A. Meneses, et al., *Appl. Catal., A* **248**, 143 (2003).
81. R. Pereniguez, V. M. Gonzalez-DelaCruz, J. P. Holgado, and A. Caballero, *Appl. Catal., B* **93**, 346 (2010).
82. G. Valderrama, A. Kiennemann, C. U. de Navarro, and M. R. Goldwasser, *Appl. Catal., A* **565**, 26 (2018).
83. G. Valderrama, A. Kiennemann, and M. R. Goldwasser, *Catal. Today* **113–135**, 142 (2008).
84. G. Valderrama, A. Kiennemann, and M. R. Goldwasser, *J. Power Sources* **195**, 1765 (2010).
85. G. Valderrama, C. U. de Navarro, and M. R. Goldwasser, *J. Power Sources* **234**, 31 (2013).
86. S. M. Lima, J. M. Assaf, M. A. Pena, and J. L. G. Fierro, *Appl. Catal., A* **311**, 94 (2006).
87. G. Amow and S. J. Skinner, *J. Solid State Electrochem.* **10**, 538 (2006).
88. M. Merz, D. Fuchs, A. Assmann, et al., *Phys. Rev. B: Condens. Matter* **84**, 014436 (2011).

89. J. R. de Paz, J. H. Velasco, M. T. Fernandez-Diaz, et al., *J. Solid State Chem.* **148**, 361 (1999).
90. H. Mao, Y. Wei, and H. Gui, *J. Appl. Phys.* **115**, 213910 (2014).
91. G. Amow, P. S. Whitfield, I. J. Davidson, et al., *Ceram. Int.* **30**, 1635 (2004).
92. Y. Toyosumi, H. Ishikawa, and K. Ishikawa, *J. Alloys Compd.* **408–412**, 1200 (2006).
93. H. Taguchi, H. Kido, and K. Tabata, *Physica A* **344**, 271.
94. W. Wong-Ng, W. Laws, K. R. Talley, et al., *J. Solid State Chem.* **215**, 128 (2014).
95. T. N. Gartman, F. S. Sovetin, E. A. Borovkova, et al., *Pet. Chem.* **55**, 455 (2015).
96. A. G. Dedov, A. S. Loktev, D. A. Komissarenko, et al., *Fuel Process. Technol.* **148**, 128 (2016).
97. A. G. Dedov, A. S. Loktev, G. N. Mazo, et al., *Dokl. Phys. Chem.* **462**, 99 (2015).
98. A. G. Dedov, D. A. Komissarenko, A. S. Loktev, et al., *Theor. Found. Chem. Eng.* **48**, 700 (2014).
99. A. G. Dedov, O. A. Shlyakhtin, A. S. Loktev, et al., *Dokl. Chem.* **484**, 16 (2019).
100. M. M. Nair and S. Kaliaguine, *New J. Chem.* **40**, 4049 (2016).
101. A. G. Dedov, A. S. Loktev, V. K. Ivanov, et al., *Dokl. Phys. Chem.* **461**, 73 (2015).
102. A. G. Dedov, A. S. Loktev, I. E. Mukhin, et al., *Pet. Chem.* **59**, 385 (2019).
103. O. Gonzalez, J. Lujano, E. Pietri, and M. R. Goldwasser, *Catal. Today* **107–108**, 436 (2005).
104. S. Zhang, J. Wang, H. Liu, and X. Wang, *Catal. Commun.* **9**, 995 (2008).
105. S. Damyanova, B. Pawelec, K. Arishtirova, et al., *Appl. Catal., B* **92**, 250 (2009).
106. S. Damyanova, B. Pawelec, R. Palcheva, et al., *Appl. Catal., B* **225**, 340 (2018).
107. K. Parkhomenko, A. Tyunyaev, L. M. Martinez Tejada, et al., *Catal. Today* **189**, 129 (2012).
108. H. Liu, S. Li, S. Zhang, et al., *Catal. Commun.* **9**, 51 (2008).
109. D. Liu, X.-Y. Quek, H. H. A. Wah, et al., *Catal. Today* **148**, 243 (2009).
110. D. Liu, W. N. E. Cheo, Y. W. Y. Lim, et al., *Catal. Today* **154**, 229 (2010).
111. B. Erdogan, H. Arbag, and N. Yasyerli, *Int. J. Hydrogen Energy* **43**, 1396 (2018).
112. S. Zhang, S. Muratsugu, N. Ishiguro, and M. Tada, *ACS Catal.* **3**, 1855 (2013).
113. M. Kaydouh, N. El Hassan, A. Davidson, et al., *C. R. Chim.* **18**, 293 (2015).
114. T. Xie, X. Zhao, J. Zhang, et al., *Int. J. Hydrogen Energy* **40**, 9685 (2015).
115. Z. Liu, J. Zhou, K. Cao, et al., *Appl. Catal., B* **125**, 324 (2012).
116. T. Xie, L. Shi, J. Zhang, and D. Zhang, *Chem. Commun.* **50**, 7250 (2014).
117. Y. H. Guo, C. Xia, and B. S. Liu, *Chem. Eng. J.* **237**, 421 (2014).
118. I. Rivas, J. Alvarez, E. Pietri, et al., *Catal. Today* **149**, 388 (2010).
119. N. Wang, X. Yu, Y. Wang, et al., *Catal. Today* **212**, 98 (2013).
120. M. M. Nair, S. Kaliaguine, and F. Kleitz, *ACS Catal.* **4**, 3837 (2014).
121. L. Xu, H. Songa, and L. Chou, *Catal. Sci. Technol.* **1**, 1032 (2011).
122. J. Newnham, K. Mantri, M. H. Amin, et al., *Int. J. Hydrogen Energy* **37**, 1454 (2012).
123. L. Xu, H. Song, and L. Chou, *ACS Catal.* **2**, 1331 (2012).
124. W. Shen, H. Momoi, K. Komatsubara, et al., *Catal. Today* **171**, 150 (2011).
125. X. Du, D. Zhang, R. Gao, et al., *Chem. Commun.* **49**, 6770 (2013).
126. Z. Bao, Y. Lu, J. Han, et al., *Appl. Catal., A* **491**, 116 (2015).
127. N. Sun, X. Wen, F. Wang, et al., *Energy Environ. Sci.* **3**, 366 (2010).
128. A. Peters, F. Nouroozi, D. Richter, et al., *Chem-CatChem* **3**, 598 (2011).
129. S. Sokolov, E. V. Kondratenko, M. Pohl, et al., *Appl. Catal., B* **113–114**, 19 (2012).
130. G. Liu, J. Zhang, Y. Xu, and Y. Sun, *Int. J. Hydrogen Energy* **43**, 15030 (2018).
131. I. V. Zagaynov, A. S. Loktev, A. L. Arashanova, et al., *Chem. Eng. J.* **290**, 193 (2016).
132. I. V. Zagaynov, A. S. Loktev, I. E. Mukhin, et al., *Mendeleev Commun.* **27**, 509 (2017).
133. I. V. Zagaynov, A. S. Loktev, I. E. Mukhin, et al., *Mendeleev Commun.* **29**, 22 (2019).
134. J.-S. Chang, S.-E. Park, and H. Chon, *Appl. Catal., A* **145**, 111 (1996).
135. A. Luengnaruemitchai and A. Kaengsilalai, *Chem. Eng. J.* **144**, 96 (2008).
136. A. N. Pinheiro, A. Valentini, J. M. Sasaki, and A. C. Oliveira, *Appl. Catal., A* **355**, 156 (2009).
137. P. Frontera, A. Aloise, A. Macario, et al., *Top. Catal.* **53**, 265 (2010).
138. J. Estephane, M. Ayoub, Kh. Safieh, et al., *C. R. Chim.* **18**, 277 (2015).
139. W. D. Zhang, B. S. Liu, C. Zhu, and Y. L. Tian, *Appl. Catal., A* **292**, 138 (2005).
140. K. A. Chalupka, W. K. Jozwiak, J. Rynkowski, et al., *Appl. Catal., B* **146**, 227 (2014).
141. P. Frontera, A. Macario, A. Aloise, et al., *Catal. Today* **218–219**, 18 (2013).
142. J. Estephane, S. Aouad, S. Hany, et al., *Int. J. Hydrogen Energy* **40**, 9201 (2015).
143. M. Abdollahifar, M. Haghghi, and M. Sharifi, *Energy Convers. Manag.* **103**, 1101 (2015).
144. C. Dai, S. Zhang, A. Zhang, C. Song, C. Shi, X. Guo, *J. Mater. Chem. A* **3**, 16461 (2015).
145. G. Moradi, F. Khezeli, and H. Hemmati, *J. Nat. Gas Sci. Eng.* **33**, 657 (2016).
146. A. I. Osman, J. Meudal, F. Laffir, et al., *Appl. Catal., B* **212**, 68 (2017).

147. M. Sharifi, M. Haghghi, and M. Abdollahifar, *J. Nat. Gas Sci. Eng.* **23**, 547 (2015).
148. A. G. Dedov, A. S. Loktev, I. E. Mukhin, et al., *Petr. Chem.* **58**, 203 (2018).
149. A. G. Dedov, A. S. Loktev, D. A. Levchenko, et al., *Theor. Found. Chem. Eng.* **49**, 502 (2015).
150. J. R. Rostrup-Nielsen and J. H. Bak Hansen, *J. Catal.* **144**, 38 (1993).
151. F. Basile, L. Basini, M. D'Amore, et al., *J. Catal.* **173**, 247 (1998).
152. A. Bhattacharyya, V. W. Chang, and D. J. Schumacher, *Appl. Clay Sci.* **13**, 317 (1998).
153. T. Shishido, M. Sukenobu, H. Morioka, et al., *Catal. Lett.* **73**, 21 (2001).
154. K. M. Lee and W. Y. Lee, *Catal. Lett.* **83**, 65 (2002).
155. A. I. Tsyganok, T. Tsunoda, S. Hamakawa, et al., *J. Catal.* **213**, 191 (2003).
156. K. Takehira, T. Shishido, P. Wan, et al., *J. Catal.* **221**, 43 (2004).
157. J. Guo, H. Lou, H. Zhao, et al., *Appl. Catal., A* **273**, 75 (2004).
158. Z. Hou and T. Yashima, *Appl. Catal., A* **261**, 205 (2004).
159. O. W. Perez-Lopez, A. Senger, N. R. Marcilio, and M. A. Lansarin, *Appl. Catal., A* **303**, 234 (2006).
160. T. P. Maniecki, K. Bawolak-Olczak, P. Mierczyński, et al., *Chem. Eng. J.* **154**, 142 (2009).
161. A. Serrano-Lotina, L. Rodriguez, G. Muñoz, and L. Daza, *J. Power Sources* **196**, 4404 (2011).
162. A. Serrano-Lotina, A. J. Martin, M. A. Folgado, and L. Daza, *Int. J. Hydrogen Energy* **37**, 12342 (2012).
163. A. Serrano-Lotina and L. Daza, *J. Power Sources* **238**, 81 (2013).
164. A. Serrano-Lotina and L. Daza, *Appl. Catal., A* **474**, 107 (2014).
165. G. de Souza, C. Ruoso, N. R. Marcilio, and O. W. Perez-Lopez, *Chem. Eng. Commun.* **203**, 783 (2016).
166. C. Tanios, S. Bsaibes, C. Gennequin, et al., *Int. J. Hydrogen Energy* **42**, 12818 (2017).
167. A. G. Dedov, A. S. Loktev, V. P. Danilov, et al., *Petr. Chem.* **58**, 418 (2018).

Translated by S. Zatonsky